NAVWEPS REPORT 8734
NOTS TP 3793
COPY 35

STRESS WAVE PASSAGE IN SELECTED ROCK FABRICS

by

Carl F. Austin
Werner Goldsmith
Stephen Finnegan

Research Department

ABSTRACT. This study is on the transmission and decay of pulses produced by impact in a very coarse-grained leucogranite, a fine-grained spessartite, and a fine-grained to aphanitic basalt.

For most tests, ballistically suspended Hopkinson bars of these rock materials, 0.845 inches in diameter and 18 inches long, were subjected to longitudinal impact by ½-inch-diameter hardened steel spheres at an initial velocity of 3,250 ± 1.5% ips. Strain gages attached to the specimens at various stations recorded the shape and velocity of propagation of the resultant wave in the rock rod. Similar experiments were performed on an aluminum alloy rod of identical size to assess the magnitude of the dispersion resulting from the three-dimensional character of the rod. The nature of the pulse transformation during passage permits an assessment of the validity of various models proposed for geologic substances in the field of seismology. Static tests on virgin and shocked rods were generally found to agree with predicted effects of stress wave passage on the rock structure. These effects include compressive-strength loss in the impact end and tensile-strength loss in the distal end as the result of oriented fractures and a general lowering of the static Young's modulus. Although these studies were conducted on rock, the general concepts developed are fully applicable to an understanding of the dynamic behavior of artificial granular brittle solids, such as explosives and concrete.

U.S. NAVAL ORDNANCE TEST STATION

China Lake, California

June 1965

U. S. NAVAL ORDNANCE TEST STATION

AN ACTIVITY OF THE BUREAU OF NAVAL WEAPONS

J. I. HARDY, CAPT., USN
Commander

WM. B. MCLEAN, PH.D.
Technical Director

FOREWORD

The material in this report represents part of an applied research program conducted in support of explosive ordnance problems at the U. S. Naval Ordnance Test Station.

The study was supported by Bureau of Naval Weapons Task Assignment RMMO-42-004/216-1/F008-08-06.

Dr. Werner Goldsmith, consultant to this Station and one of the co-authors of this report, is a Professor of Engineering at the University of California, Berkeley.

Released by
JOHN PEARSON, Head,
Detonation Physics Group
4 March 1965

Under authority of
HUGH W. HUNTER, Head,
Research Department

NOTS Technical Publication 3793
NAVWEPS Report 8734

Published by.....Research Department
Collation.....Cover, 34 leaves, abstract cards
First printing.....220 numbered copies
Security classification.....UNCLASSIFIED

CONTENTS

ACKNOWLEDGMENT

The dynamic tests described in this report were conducted by C. C. Wang at the University of California, Berkeley, with the assistance and supervision of the authors of this report. Mr. Wang's work was submitted as a thesis in partial fulfillment of the requirements for the M.S. degree (in Mechanical Engineering) in October 1964.

INTRODUCTION

Rocks, in contrast to metals, are generally regarded as brittle, macroscopically inhomogeneous, anisotropic materials. As a consequence, the reproducibility of tests for the determination of the physical properties of rocks has frequently been questioned. However, as shown in a previous study, the careful selection and treatment of rock specimens can greatly reduce the degree of variation in experimental data (Ref. 1). If rock specimens are chosen from the same rock classification, the same general geographic location, and with the same general structural orientation within the source mass, the subsequent test results will be as consistent as for metals of a specific composition and prescribed mechanical and thermal treatment. In addition, care is required to ensure that all rock samples to be compared receive the same handling and preparation because rocks are very sensitive to damage due to shock or vibration. These precautions are no more complex than those faced by the user of metal samples, who must provide complete specifications including even the company of origin when detailed test correlations are desired.

A previous investigation on diorite, a typical granitic igneous rock, was concerned with stress pulse propagation in a Hopkinson bar loaded by the central longitudinal impact of a steel sphere. Very interesting differences were observed between the initial shape and subsequent metamorphosis of the pulse during passage along the rock rod and the corresponding behavior in an aluminum rod of the same size, tested under identical conditions. In view of this observed disparity, the present investigation was conducted to determine if these differences could also be found in other rock fabrics. To decrease the number of variables, the tests were limited to igneous rocks of various grain sizes and compositions. As in the case of diorite, an analysis of the test results was carried out to attempt the construction of a simple phenomenological model of material behavior. Static tests were conducted on both virgin and shocked specimens to assess the effect of stress wave passage in the various rock fabrics employed.

Three different igneous rocks, spessartite, basalt, and leucogranite, were employed in this investigation. Pertinent results from the previous studies in diorite are included in the discussions for completeness. These rocks represent a wide spectrum of common igneous fabrics, involving large differences in texture and composition. As a standard, specimens of aluminum alloy 2024 T-4 were tested under the same conditions to establish the magnitude of the dispersive effect for a longitudinal pulse in an elastic rod of identical diameter.

SUMMARY OF PREVIOUS WORK

Stress waves in solids at nominal stress levels may be divided into three major classes: elastic, viscoelastic, and plastic. The mathematical theory of stress wave propagation in elastic solids was developed by Pochhammer, Chree, Rayleigh, Kelvin, and others during the latter part of the 19th century (Ref. 2 and 3). After that, the field remained virtually untouched for three decades, with the exception of a few scattered papers. After 1930, some signs of revival began to appear and during the 1940's, various significant developments occurred including the advancement of theories of plastic wave propagation by Kármán, Taylor, and other investigators (Ref. 4–6). After 1950, steadily increasing attention was devoted to this area and both general theory and experimental techniques were covered in a number of books and survey papers (Ref. 7–13).

The Hopkinson pressure bar test was first initiated by Hopkinson in 1914, and then further developed by Robertson in 1921, and by Landon and Quinney in 1923 (Ref. 14 and 15). In 1948, Davies critically examined and further improved this test, which has since developed into a method frequently used in finding the dynamic properties of materials (Ref. 16). Using the Hopkinson pressure bar principle, Rinehart found the dynamic tensile strength of mild steel, Kolsky and Shi tested glass and plastics, and Bacon determined the dynamic tensile strength of basalt and sandstone (Ref. 17–20).

Fracturing of rock by means of explosively generated high-amplitude pulses has been studied by Grine who found that the high porosity in rock produced a large attenuation effect that resulted in destruction of the porous test material at stress levels much smaller in relation to their static strength than for nonporous rocks (Ref. 21). As examples, a graywacke with 0.15% porosity was not damaged by a compressive pulse with an axial stress of 6.7 times the static compressive strength of the rock, but more porous media such as limestone (0.8%) and concrete (3%) were destroyed by dynamic axial stresses with amplitudes less than 2 times the static strength of the materials.

Bruckshaw and others determined the variation in elastic constants for sandstone, oolitic limestone, shelly limestone, granite, dolerite, and diorite in the frequency range of 40–120 cps (Ref. 22). Differences of 2 to 2.6% were observed in the dynamic elastic constants between the two extremes of frequency employed. The variations tended to increase at lower frequencies and to decrease at higher frequencies. At higher frequencies, the frictional loss of energy per cycle $\Delta u/u$ was essentially independent of frequency while the harder, more compact rocks, such as the igneous rocks, had lower values of $\Delta u/u$.

Attewell has studied the response of rocks to high stress levels using explosives as the energy source (Ref. 23). Attewell's results were based on the use of thin cylindrical slices of rock placed between two portions

of a Hopkinson bar of metal and upon the use of long rods of rock in a Hopkinson-bar configuration. Stress-strain and strain-time curves were obtained from the long rods using radial and parallel capacitance gages. Two dolomites, Tunstead limestone, Darley Dale sandstone, Carrara marble, and granodiorite were tested, and the results indicated to Attewell that the rocks exhibited a viscoelastic behavior that included considerable nonrecoverable hysteresis during the priod of the incident pulse.

THEORETICAL CONSIDERATIONS

WAVE PROPAGATION IN AN ELASTIC BAR

The propagation of pulses in a circular elastic bar of infinite extent has been analyzed by Pochhammer and Chree according to the exact, axisymmetric equations of elastodynamics (Ref. 2 and 3). Three types of waves were found to exist for harmonic pulses: longitudinal or symmetric, flexural or antisymmetric, and torsional, and each exhibits an infinite spectrum of modal shapes. More recent theoretical investigations have also pointed to the possibility of the presence of coupling among these kinds of wave types, to the existence of coupling among several modes of a single wave type, and to the possible occurrence of complex wave numbers, which characterize a transient with an amplitude depending upon position (Ref. 24 and 25). Comparable solutions have not been obtained for a bar of finite length, nor for the case of transient pulse propagation. Despite this, the Pochhammer-Chree relations have been employed as a standard in the examination of wave phenomena on the basis that pulse propagation in finite bars should embody most of the essential characteristics of wave propagation in the infinite model. Thus, predictions of the propagation of nonharmonic transients could be accomplished either by the superposition of its harmonic constituents as obtained by a Fourier analysis of the pulse, or by the method of stationary phase that traces certain aspects of pulse propagation on the basis of interference and reinforcement of various harmonics (Ref. 16).

The examination of numerous experimental results has indicated that separation of the components of these types of waves is possible by proper methods of pulse generation and measurement. In addition, the test bars will principally respond in the fundamental mode of motion of one or more of the previously cited wave-types in virtually all physical situations. The Pochhammer-Chree relations indicate that longitudinal waves propagating in any bar of finite diameter will disperse. Thus each harmonic component of such a wave will propagate with its own characteristic velocity c that depends only on the rod radius, a, and the wave length, λ, or alternatively the frequency, ω. With these concepts, a dispersion curve can be constructed as shown in Fig. 1 for the first three modes of longitudinal motion, providing a ratio of the phase velocity, c, to "rod"

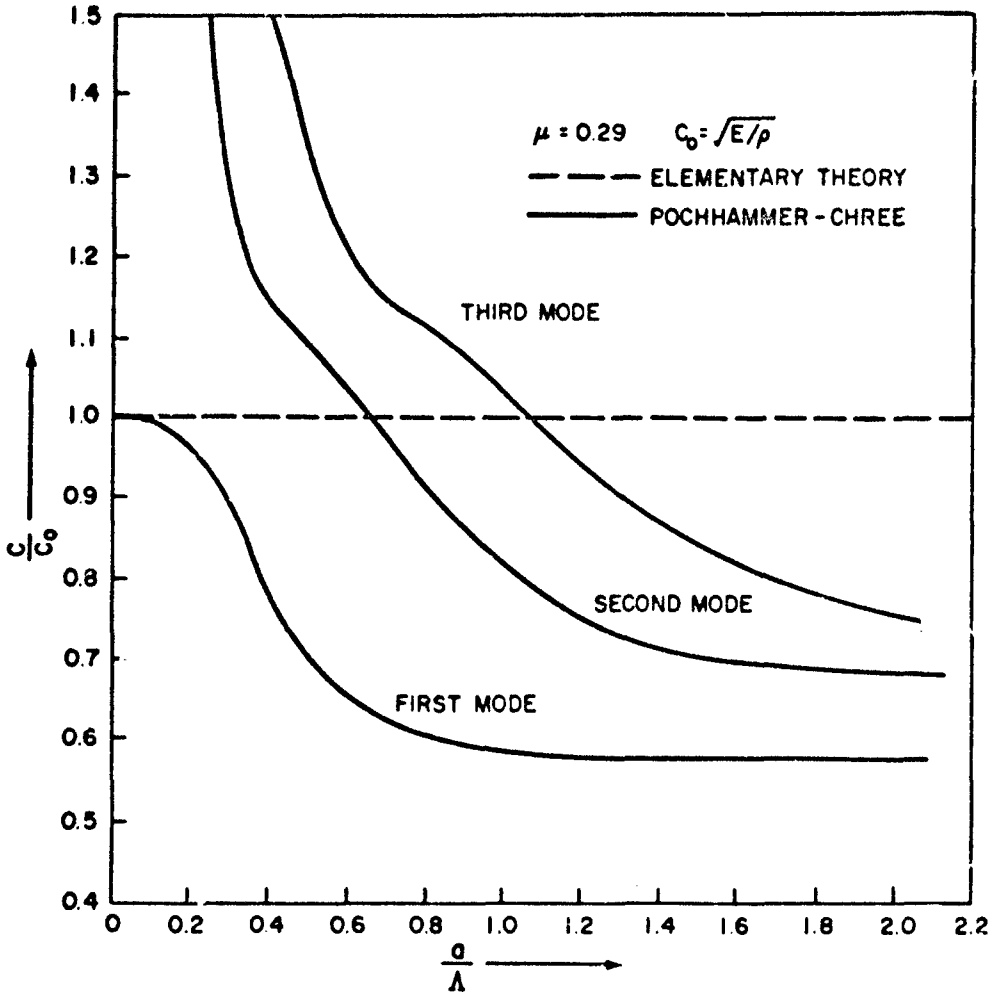

FIG. 1. Phase Velocity of Longitudinal Waves in Cylindrical Rods of Infinite Length (Ref. 15).

velocity, $c_o = \sqrt{E/\rho}$, where E is Young's modulus, and ρ is the mass density in terms of the ratio a/λ of a particular harmonic component.

In principle, the analysis of the propagation of waves in an elastic bar is possible by means of this exact theory but the mathematical complexities involved render such a treatment virtually impossible for the reduction of experimental results. Instead, such data are usually analyzed by means of a one-dimensional theory. The case of longitudinal motion is of principal interest and results in the following well-known equation:

$$c_o^2 \frac{\partial^2 u}{\partial x^2} = \frac{\partial^2 u}{\partial t^2} \quad \text{or} \quad c_o^2 \frac{\partial^2 \sigma}{\partial x^2} = \frac{\partial^2 \sigma}{\partial t^2} \tag{1}$$

where u and σ are the longitudinal displacement and stress, and x and t are the coordinate in the direction of propagation and time, respectively. Equation 1 is based on the assumptions that plane cross sections remain plane, that the stress distribution is uniform across the rod, and that the effects of radial inertia and transverse shear can be neglected. One-dimensional equations of motion incorporating the last two effects have also been developed, resulting in correspondingly more complicated relations.

Equation 1 predicts the propagation of a pulse without dispersion, where each harmonic component propagates with the same bar velocity c_o. The utility of the Pochhammer-Chree relations arises from the possibility of gaging the validity of the elementary theory with respect to dispersion. By performing a Fourier analysis of a typical pulse, the frequency of the harmonic component of largest energy content can be determined and a maximum bar size ascertained that can be used with any desired small amount of dispersion of this component.

Although the higher harmonics of the pulse will exhibit a greater degree of such dispersion, their corresponding affect on changes in the pulse shape will be minimized due to their relatively much lower amplitude. Thus, the elementary theory can be employed for the pulse analysis with a predetermined margin of error.

A pulse analysis was carried out for the strain-time curve obtained at station G-1, shown in Fig. 17 in a later section, which represents the shortest pulse duration encountered and is, therefore, the most sensitive with regard to dispersive effects. From Fig. 1, a maximum value of $a/\lambda = 0.08$ is obtained in order that the phase velocity ratio c/c_o be greater than 0.99. For the run being used as an example, the observed period of the main portion of the pulse T, was 30 μsec, and the corresponding measured rod velocity c_o was 231,000 ips. With this information, the maximum permissible rod radius for this amount of dispersion can be obtained as follows:

$$a_{max} = Tc_o\,(a/\Lambda)(c/c_o)$$

$$= 30 \times 10^{-6} \times 231{,}000 \times 0.08 \times 0.99$$

$$= 0.549 \text{ inches}$$

Thus a rod diameter of 1.098 inches would be fully acceptable for this amount of dispersion. In the present investigation, the maximum rod diameter employed was 0.845 inches, indicating that in the spessartite, with $a_{max} = 0.549$, and in the aluminum, with $a_{max} = 0.485$ inches, the amount of dispersion for the fundamental component in both materials was less than 1%. Although shorter wavelength components will be subject to greater dispersion, this problem is far less serious than if a greater tolerance had been permitted for the fundamental harmonic. If a period of 2 T is employed to more accurately represent the pulse in a symmetrical form, as shown in Fig. 2, an even lower magnitude of the dispersive effect is obtained. From these indications, the elementary theory can be reasonably applied in the present studies with a relatively small amount of distortion due to geometrical dispersion, which is of vital importance in the analysis of the data.

SIMPLE MACROSCOPIC MODELS OF MATERIAL BEHAVIOR

The preceding description of the propagation of longitudinal elastic waves is a good approximation for the propagation of this type of transient pulse in most metals, especially in the type of aluminum used in the calibration bar, providing the yield point of the material is not exceeded. The mechanical model of such a substance is a simple linear spring, with the corresponding constitutive equation given by the one-dimensional stress-strain relation

$$\sigma = E\epsilon \qquad (2)$$

where σ is stress, and ϵ is strain. Other types of substances, including most natural materials, exhibit time-dependent or dissipative mechanisms including internal friction, and require the stipulation of a more comprehensive constitutive relation to account for the loss of energy during stress wave passage.

One of the principal aims of the present investigation is the delineation of an appropriate model for the various rocks tested. For those not familiar with this subject, some of the more common mechanisms that have been used to represent various groups of nonmetallic substances are briefly described and discussed.

The most frequently employed anelastic model for geological materials is the Kelvin-Voigt solid, which is a two-element viscoelastic system and is represented by the spring-dashpot configuration shown in Fig. 3. The

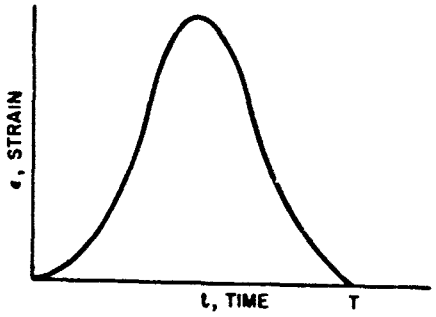

(a) Actual Pulse Shape.

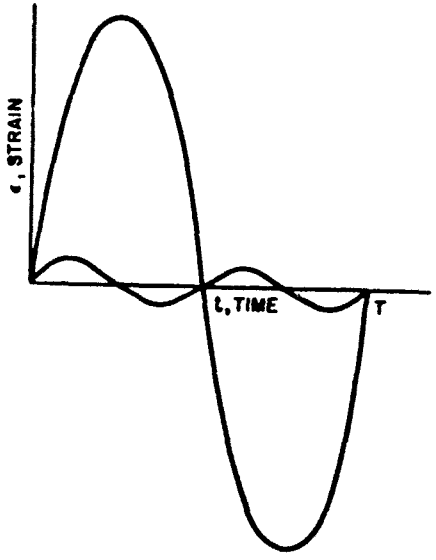

(b) Fourier Analysis Based on T.

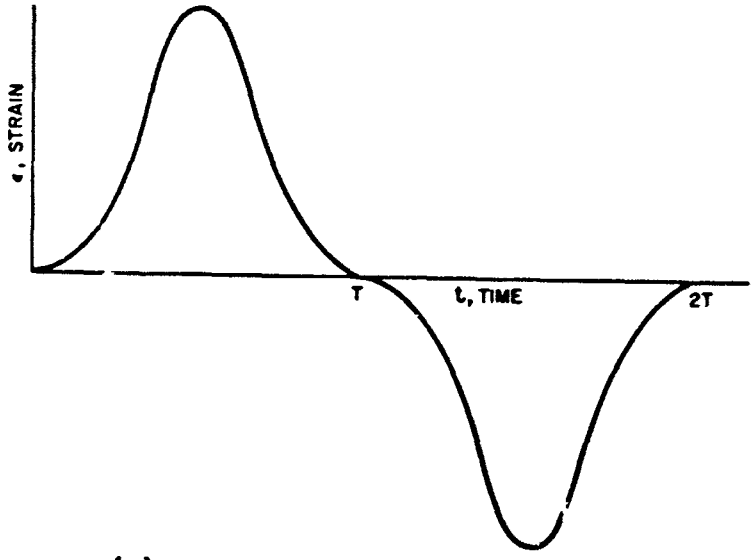

(c) Pulse Shape and Mirror Image.

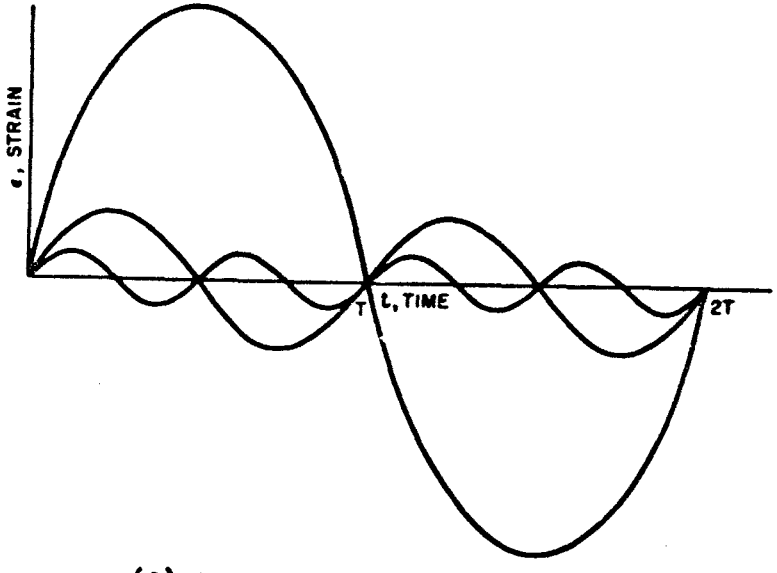

(d) Fourier Analysis Based on 2T.

FIG. 2. Fourier Analysis of a Wave Comparing Results With Periods T and 2T.

one-dimensional constitutive equation and the corresponding relations for one-dimensional wave propagation for this type of material are given by the following equations:

$$\sigma = E_1 \epsilon + \eta_1 \frac{d\epsilon}{dt} \tag{3}$$

$$\frac{\partial^2 u}{\partial x^2} + \frac{\eta_1}{E_1} \frac{\partial^3 u}{\partial x^2 \partial t} = \frac{1}{c_o^2} \frac{\partial^2 u}{\partial t^2} \tag{4}$$

The spring constant E_1 and the viscous damping coefficient η_1 are assumed to be constant for a given substance. The equation of motion (Eq. 4) is satisfied by a plane harmonic component of the form:

$$u = U_o e^{-\alpha x} e^{i(pt - fx)} \tag{5}$$

where p is the natural frequency and f is the wave number. The foregoing is proper provided the phase velocity $c = p/f$ and the attenuation coefficient α are determined by the relations:

$$\left(\frac{c}{c_o}\right)^2 = \frac{2}{\xi^2}\left[(1 + \xi^2)(\sqrt{1 + \xi^2} - 1)\right] \quad \text{with } \xi = \frac{p\tau_1}{E_1} \tag{6}$$

and

$$\alpha = \frac{p}{c}\left[-1 + \sqrt{1 + \xi^2}\right] \tag{7}$$

For values of $\xi \ll 1$, $c/c_o \to 1$ and $\alpha \to (\eta_1 p^2)/(2c_o E_1)$, the equations yield attenuation proportional to the square of the frequency of the component without dispersion and for large values of ξ, $c/c_o \to \sqrt{(2\tau_1 p)/(E_1)}$ and $\alpha \to 1/c_o \sqrt{(E_1 p)/(2\tau_1)}$, the equations describe a dispersive propagation. The Kelvin-Voigt solid has been investigated under a variety of initial and boundary conditions but the only real rock material found thus far which approximates the attenuation and dispersion requirements for this model is the Pierre shale of eastern Colorado (Ref. 26-28).

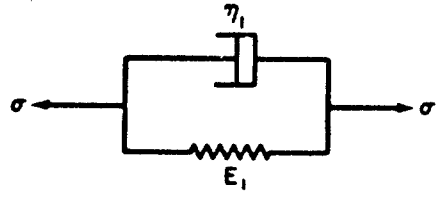

σ = APPLIED STRESS
E_1 = SPRING CONSTANT
η_1 = VISCOUS DAMPING COEFFICIENT

FIG. 3. Kelvin-Voigt Solid.

Another two-element viscoelastic body is represented by the Maxwell solid as shown in Fig. 4. The one-dimensional constitutive equation and one-dimensional wave equation for the Maxwell solid are as follows:

$$\sigma + \frac{\eta_1}{E_1}\frac{d\sigma}{dt} = \eta_1 \frac{d\epsilon}{dt} \tag{8}$$

$$\frac{\partial^2 u}{\partial x^2} = \frac{1}{c_o^2}\left(\frac{\partial^2 u}{\partial t^2} + \frac{E_1}{\eta_1}\frac{\partial u}{\partial t}\right) \tag{9}$$

where E_1 and η_1 are again constants. Equation 9 is satisfied by a harmonic component of the form given by Eq. 5 provided that

$$\left(\frac{c}{c_o}\right)^2 = 2\xi^2\left[\sqrt{1 + 1/\xi^2} - 1\right] \text{ with } \xi = \frac{p\eta_1}{E_1} \tag{10}$$

and

$$\alpha = \frac{p}{\sqrt{2}c_o}\left[\sqrt{1 + 1/\xi^2} - 1\right]^{\frac{1}{2}} \tag{11}$$

Dispersion occurs for values of $\xi \ll 1$, $c/c_o \to (2\eta_1 p)/(E_1)$ and $\alpha \to p/c_o$ while dispersion is absent with $\xi \gg 1$, $c/c_o \to 1$, and $\alpha \to E_1/2\eta_1 c_o$ and the attenuation coefficient remains constant. To date, no geologic material has been found that is reasonably well represented by the Maxwell model.

σ = APPLIED STRESS
E_1 = SPRING CONSTANT
η_1 = VISCOUS DAMPING COEFFICIENT

FIG. 4. Maxwell Solid.

A combination of the Kelvin-Voigt and Maxwell models leads to the standard linear solid shown in Fig. 5. The constitutive relations for this material are given by

$$\sigma + \frac{\eta_1}{E_1}\frac{d\sigma}{dt} = E_2\epsilon + \frac{\eta_1}{E_1}(E_1 + E_2)\frac{d\epsilon}{dt} \tag{12}$$

or, alternatively, by

$$\sigma = E_2\epsilon + E_1\int_0^t e^{\frac{-E_1(t-\tau)}{\eta_1}} \frac{d\epsilon}{d\tau}\, d\tau \tag{13}$$

where τ is variable of integration. A generalization of the standard linear solid, accounting for nonlinear behavior, is known as the Boltzman model. This model is mathematically described by the relation

$$\sigma = f(\epsilon) + \int_0^t \phi(t-\tau)\frac{d\epsilon}{d\tau}\, d\tau$$

The characteristic constants or functionals occurring in the equations of material behavior are normally obtained from creep, relaxation, and steady-state dynamic load tests.

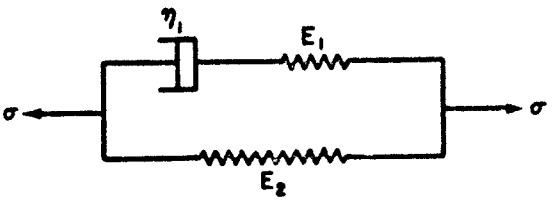

σ = APPLIED STRESS
E_1, E_2 = SPRING CONSTANT
η_1 = VISCOUS DAMPING COEFFICIENT

FIG. 5. Standard Linear Model.

A model that seems to hold high promise for a reasonably accurate description of the major features of many geologic materials is the representation involving structural damping shown in Fig. 6 (Ref. 29 and 30). In this model, the damping force is given by Ehx with h being a nondimensional constant. The constitutive relation for harmonic components and the wave equation for the one-dimensional case are now given by:

$$\sigma = E_1\epsilon + \frac{E_1 h}{|p|}\frac{d\epsilon}{dt} \tag{14}$$

and

$$\left[1 + \frac{h}{|p|}\frac{\partial}{\partial t}\right]\frac{\partial^2 u}{\partial x^2} = \frac{1}{c_o^2}\frac{\partial^2 u}{\partial t^2} \tag{15}$$

In these equations the absolute value of frequency, p, is utilized to take care of both positive and negative components of the Fourier spectrum of the pulse. Equation 15 is satisfied by the wave form represented by Eq. 5 and propagates without dispersion with a phase velocity c, given by:

$$\frac{c}{c_o} = \frac{1}{\gamma}\left[1 + h^2\right]^{\frac{1}{2}} \quad \text{where} \quad \gamma = \left[\frac{1}{2}\left(1 + \sqrt{1 + h^2}\right)\right]^{\frac{1}{2}} \tag{16}$$

The attenuation coefficient α is, however, frequency dependent and is given by:

$$\alpha = \frac{\phi p}{c}\left[1 + h^2\right]^{\frac{1}{2}} \quad \text{with} \quad \phi = \left[\frac{1}{2}\left(-1 + \sqrt{1 + h^2}\right)\right]^{\frac{1}{2}} \tag{17}$$

These equations reduce to ordinary elastic wave propagation for $h \ll 1$, $c/c_o \to 1$, $\alpha \to 0$. The previously reported investigations in diorite have shown that pulse propagation in a dioritic material conforms well to the nondispersive character of this model.

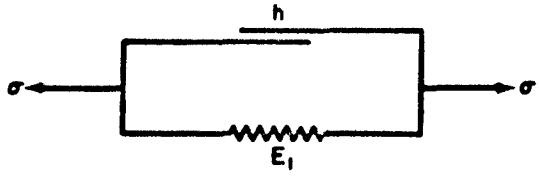

σ = APPLIED STRESS
E_1 = SPRING CONSTANT
h = NONDIMENSIONAL CONSTANT

FIG. 6. Structural Damping Model.

Other types of solids utilized in studies of this type include the St.-Venant model, shown in Fig. 7, the four-element model shown in Fig. 8, and the Bingham model shown in Fig. 9. The St.-Venant model entails strain which is linearly elastic until the attainment of a critical value, the yield strain, beyond which the model provides perfectly plastic behavior. The four-element mechanism provides for instantaneous and delayed elasticity and viscous flow and consists of the coupling in series of a Kelvin-Voigt and a Maxwell solid. The Bingham model is a modification of the St.-Venant configuration and acts as an elastic body below the yield point, but for loads in excess of the yield point a constant load produces a steadily increasing strain.

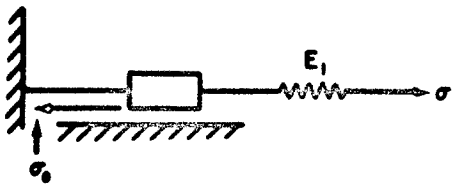

σ = APPLIED STRESS
σ_0 = YIELD STRESS
E_1 = SPRING CONSTANT

FIG. 7. St.-Venant Model.

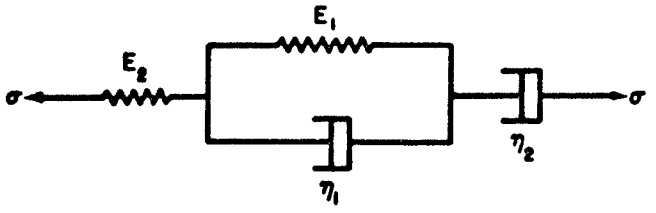

σ = APPLIED STRESS
E_1, E_2 = SPRING CONSTANT
η_1, η_2 = VISCOUS DAMPING COEFFICIENT

FIG. 8. Four-Element Model.

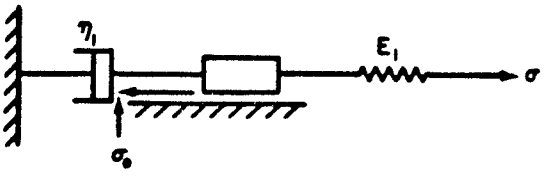

σ = APPLIED STRESS
σ_0 = YIELD STRESS
η_1 = VISCOUS DAMPING COEFFICIENT
E_1 = SPRING CONSTANT

FIG. 9. Bingham Model.

SELECTION AND PREPARATION OF TEST SAMPLES AND THEIR GENERAL PHYSICAL PROPERTIES

Test materials for this experimental program were chosen to represent igneous rock fabrics that are common on a world-wide basis. Four materials, basalt, spessartite, diorite, and leucogranite, were selected that range from very fine-grained to quite coarse-grained textures. All of these rocks have the same gross mineralogic structure and all exhibit the same general mode of grain-to-grain bonding. They are also similar in chemical composition except for the leucogranite, which is potassic. By restricting the present study to igneous rocks, the petrologic variables are sharply reduced from situations where mixtures of sedimentary and metamorphic fabrics are compared with igneous rocks.

SAMPLE PREPARATION

All of the sample rocks were collected from field outcrops within the confines of the U. S. Naval Ordnance Test Station at China Lake, California. To prevent structural damage to the samples as the result of sledging or blasting, only natural boulders of the proper size were selected. To avoid material damaged by weathering and temperature cycling, the outer portions of the boulders were removed by diamond sawing.

Test specimens were obtained from the resulting blocks by means of conventional core drilling, using care to avoid excessive heating or vibration of the sample. Transportation of the sample rods from the preparation laboratory at China Lake to the dynamic test laboratory at Berkeley was controlled to prevent accidental shocks previous to impact testing.

All test rods were cut to their finished diameter of 0.845 - 0.003 inches when initially core drilled. The ends of the test rods were faced perpendicular to the longitudinal axis of the rod to yield a standard length of 18 inches, except for a few rods cut to a length of 14 inches. Additional extension pieces were provided to lengthen some of the rods, serving either as frontal protectors or as wave traps at the distal end. The frontal protectors were used to permit repeated collisions for the same rod without shortening due to impact end shattering. The wave traps were used to minimize reflected pulse interference at the distal-end strain-gage station and also to prevent fractures in the distal portion of the rods. Although the frontal pieces were usually of the same material as the test rod, some aluminum was also used. In repeated shocking of a single rod, the impact end was refaced after each collision to remove the fractured portion. Both the frontal protectors and the wave traps were connected to the test rods by means of Eastman 910 glue.

Static compression test samples of virgin rock were obtained by core drilling in the same manner as the long test rods. Compressive static tests were carried out on a standard laboratory testing machine. The ends of the compressive samples were ground parallel to each other with a deviation of 0.0005 inches across the 0.643-inch sample diameter, using 50-micron grit. The loading rate for compressive testing was 200 lb/sec. The corresponding strain was recorded by means of an extensometer. The use of an extensometer between press platens occasionally yielded inexplicable random high values, which were eliminated by measuring between the sample ends rather than between the platens.

Tensile test samples were also obtained by diamond drill coring, using either the test-rod diameter, or in the case of very strong and uniform materials, a smaller sample diameter. Tensile tests consisted of joining the test cylinder to small steel holders with HYSOL Epoxy Patch Kit 6-C. The upper holder was attached to an overhead beam by a cable and the lower carried a freely suspended pan, which was loaded with lead shot. Loading was at 25 lb/min in 25-pound increments, which permitted some indication of the time effects on the ultimate strength of the rock materials.

MATERIALS

BASALT. A basalt is defined as an extrusive rock with 5–50% dark minerals; a plagioclase feldspar with a composition of labradorite to bytownite; a total quartz and feldspar content that is less than 5% quartz; and a total feldspar content that is less than 5% potash feldspar. The basalt employed as a test material in this study has a density of 2.72 g/cc and consists of medium-grained to fine-grained phenocrysts (0.5–1 mm) set in an extremely fine-grained to glassy ground mass (less than 0.05 mm). This material, based on phenocryst composition, is 10% dark minerals, has a plagioclase with the composition of labradorite, and contains no potash feldspar. The basalt employed in these tests is described in detail as Sample 62 in Ref. 31.

To ensure a reasonable degree of uniformity in the basaltic samples, all core specimens for the dynamic tests were taken parallel to the flow plane of the basalt and in a direction nearly perpendicular to the flow direction as indicated by the alignment of the feldspar laths. Static test cores were also taken in three mutually perpendicular directions, one of which was the dynamic test direction. The static test results for fresh basalt are shown in Table 1.

The static tensile strength for the virgin basalt is in the range of 1,100–1,700 psi, with an average of 1,400 psi for the samples taken from a direction parallel to the test rods. The static compressive strength of the virgin basalt is in the range of 33,900–41,200 psi with an average 37,000 psi, and with a length-to-diameter ratio of approximately 1.5. Although the three directions tested had similar static compressive

TABLE 1. Static Strengths of Virgin Basalt Cores

Orientation	Length, in.	Diam., in.	Area, $in.^2$	Compressive strength		Young's modulus, psi x 10^{-6}	Tensile strength			
				Load at failure, lb	Stress at failure, psi		Diam., [a] in.	Area, $in.^2$	Load at failure, lb	Failure, psi
Parallel to test rods	1.245	0.843	0.558	23,000[b]	41,200	...	0.238	0.0445	50-75[c]	1,400
	1.2455	0.8435	0.559	21,200	37,900	7.2	.....	.....	...	.....
	1.243	0.843	0.558	17,800	31,800	5.8	0.238	0.0445	75	1,700
	1.245	0.845	0.561	22,000	39,200	...	0.238	0.0445	50[d]	1,100
Perpendicular to test rods	1.245	0.843	0.558	21,600	38,600	3.4	0.239	0.0449	50[d]	1,100
	1.2435	0.8405	0.555	18,800	33,900	2.9	0.239	0.0449	50[d]	1,100
	1.243	0.840	0.554	22,700	41,000	...	0.239	0.0449	50[d]	1,100
	1.2425	0.843	0.558	19,200	34,800	2.4	.....	.....	...	.....
Perpendicular to preceding two test directions	1.244	0.842	0.557	21,300	38,200	2.7	0.238	0.0445	50-75[c]	1,400
	1.244	0.8425	0.557	19,900	35,700	2.3	.....	.....	...	.....
	1.243	0.843	0.558	22,500	40,300	2.6	0.239	0.0449	50[d]	1,100
	1.2435	0.842	0.557	21,500	38,500	2.2	0.239	0.0449	50[d]	1,100

[a] Sample lengths for tensile tests are 0.5 in.
[b] Unknown loading rate, but quite rapid, about 600 lb/sec.
[c] Between these numbers.
[d] Sample failed after 3-5 sec wait.

strengths, their values for Young's modulus varied significantly. Larger values of Young's modulus, with an average of 6.5×10^6 psi, were found for the specimens taken from a direction parallel to the test rods. Basalt is used as an example of a fine-grained to aphanitic igneous rock.

SPESSARTITE. Spessartite is defined as a dike rock composed of 5–50% dark minerals and plagioclase with a composition of oligocene to bytownite. The total feldspar content is less than 5% potash feldspar. The spessartite employed as a test material is composed of 40% dark minerals, has labradorite as the plagioclase, and contains negligible amounts of quartz and potash feldspar. This rock has a density of 2.89 g/cc and the grain structure exhibits no gross orientation upon microscopic examination. The grain size for the rock as a whole is from 0.4–0.8 mm, which is intermediate to the fine-grained extrusive rocks such as basalt and medium- to coarse-grained intrusive rucks such as diorite and leucogranite. This spessartite, which occurs in dikes, has been described as Sample 41 in Ref. 31.

To ensure a reasonable degree of uniformity in the samples, all core specimens for the dynamic tests were taken parallel to the dike and in a vertical direction. Static test cores were taken from three mutually perpendicular directions, one of which was the same as that of the dynamic test samples, and the other two were taken horizontally in directions parallel and perpendicular to the dike plane. The test results for samples of fresh spessartite are shown in Table 2.

The values for Young's modulus and the tensile strength of the spessartite were variable, although the static compressive strength was quite uniform, with the highest values being obtained in the dynamic-test-rod direction. The static tensile strength ranged from 1,100–3,100 psi and averaged about 2,500 psi. The static compressive strength of virgin spessartite averaged 54,000 psi, and Young's modulus varied from 4.6 to 11.4×10^6 psi, depending on orientation. The average static compressive strength and static Young's modulus of the test direction are slightly higher than the values for the other two directions tested. Spessartite is used as an example of a fine- to medium-grained igneous rock.

DIORITE. Diorite is defined as an intrusive rock composed of 5–50% dark minerals, containing a plagioclase with a composition of oligoclase to andesine, exhibiting a total feldspar content containing less than 5% potash feldspar, and with a total quartz and feldspar content comprised of less than 5% quartz. The samples of diorite used to form the test specimen contain 20% dark minerals, andesine plagioclase, a total quartz and feldspar content comprised of 3–5% quartz, and a feldspar content with less than 3% potash feldspar. The diorite grain size is typical for intrusive rocks. Scattered mineral grains occasionally reach 5–6 mm in length, but the average for the rock is closer to 1–2 mm. The diorite has been described in detail as Sample 84 in Ref. 31, and the static properties of the diorite have been discussed in previous studies (Ref. 1). In summary, the diorite employed has a

TABLE 2. Static Strengths of Virgin Spessartite Cores[a]

Orientation	Length, in.	Diam., in.	Area, in.^{2}	Compressive strength		Young's modulus, psi x 10^{-6}	Tensile strength			
				Load at failure, lb	Stress at failure, psi		Diam., in.	Area, in.^{2}	Load at failure, lb	Failure, psi
Parallel to test rods, plane of dike	1.240	0.845	0.560	30,500	54,500	8.9	0.238	0.0445	100-125	2,500
	1.240	0.845	0.560	30,300	54,200	11.2	0.238	0.0445	100-125	2,500
	1.240	0.845	0.560	30,000	53,600	5.7	0.238	0.0445	100-125	2,500
	1.247	0.845	0.560	29,600	52,900	7.4				
	1.298[b]	0.845	0.560	31,500[c]	56,300	11.4				
	1.298[b]	0.845	0.560	32,200[d]	57,500	8.8				
	1.298[b]	0.845	0.560	31,100[c]	55,500	...				
Perpendicular to test rods and to plane of dike	1.248	0.845	0.560	29,400	52,500	7.1	0.238	0.0445	50-75	1,400
	1.240	0.845	0.560	30,000	53,500	4.6	0.238	0.0445	100-125	2,500
	1.242	0.845	0.560	30,400	54,400	7.4	0.238	0.0445	125-150	3,100
	1.240	0.845	0.560	28,800	51,500	5.5				
Perpendicular to test rods and parallel to plane of dike	1.240	0.845	0.560	29,100	52,000	7.0	0.238	0.0445	50-75	1,400
	1.248	0.845	0.560	28,300	50,500	6.6	0.238	0.0445	100-125	2,500
	1.247	0.845	0.560	28,300	50,500	6.8	0.238	0.0445	50[e]	1,100
							0.238	0.0445	75	1,700
							0.238	0.0445	75-100	2,000
							0.238	0.0445	100	2,200

[a] Same rock rod not used in both tests.
[b] Samples reground to parallelity of better than 0.001 in. across a diameter.
[c] Loading rate of 6,000 lb/min.
[d] Loading rate of 12,000 lb/min.
[e] Sample failed after 40 sec.

density of 2.83 g/cc, a compressive strength of 32,000 psi ± 2.2%, a tensile strength of 800 psi, and a static Young's modulus of 5.06×10^6 psi ± 1%. Diorite is used as an example of a medium- to coarse-grained igneous rock.

LEUCOGRANITE. Leucogranite is the varietal term used to designate a granite with less than 5% dark minerals. Granites are defined as intrusive rocks that contain 5–50% dark minerals, a plagioclase feldspar with a composition of oligoclase to andesine, a feldspar content that is 65–95% potash feldspar, and a total quartz and feldspar content that is 5–50% quartz. The leucogranite selected as a test material has been described as Sample 53 in Ref. 31. The leucogranite has a density of 2.59 g/cc and an average grain size of 5–6 mm. The leucogranite contains 3–4% dark minerals, a total quartz and feldspar content that is 20% potash feldspar and 3–5% oligoclase.

The static tensile strength of the virgin leucogranite was found to be the lowest of any recorded for the materials tested in this study, being in the range of 330–660 psi. The large percentage variations for the tensile strengths observed can be attributed to the large grain size, the abundance of cleavage planes, and the general sensitivity of the strength of this material to geologic and mineralogic flaws and to handling damage. The static compressive strength of the virgin leucogranite averages about 30,000–33,000 psi, with the lower value referring to specimens cut parallel to the test-rod direction. Young's modulus for virgin leucogranite varied from 3.4 to 7.1 x 10^6 psi. The static test results for fresh leucogranite are shown in Table 3.

INSTRUMENTATION AND PROCEDURE

The ballistic arrangement for the Hopkinson pressure bar test is shown in Fig. 10, and a schematic diagram of the experimental setup is shown in Fig. 11. The principal equipment employed for the tests in this study consists of an air gun; two Tektronix Type 565 dual-beam oscilloscopes; two Tektronix Type 535 single-beam oscilloscopes; associated amplifiers flat from d.c. to more than 1 Mc; a detection unit for the passage of the projectile at two stations involving two minilights, two photocells and pulse shapers; and a Beckman model 7360 time interval meter with a resolution of 1 μsec.

An air gun with a pneumatic trigger was used; the air pressure was adjustable and controlled the initial projectile velocity. Steel spheres with a hardness of R_c 67, a weight of 8.35 grams and a diameter of ½ inch were employed as projectiles; their velocity was generally maintained at 3,250 ± 1.5% ips. In two cases, one half of this velocity was used. Two slots were cut in the gun barrel near the muzzle end to dissipate the propelling air charge, thus preventing further projectile acceleration,

TABLE 3. Static Strengths of Virgin Leucogranite Cores[a]

Orientation	Length, in.	Diam., in.	Area, $in.^2$	Compressive strength		Young's modulus, psi x 10^{-6}	Diam., in.	Area, $in.^2$	Tensile strength	
				Load at failure, lb	Stress at failure, psi				Load at failure, lb	Failure, psi
Parallel to test rods	1.298	0.844	0.56	15,800	28,300	3.4	0.764	0.459	275[b]	600
	1.297	0.844	0.56	16,300	29,100	...	0.764	0.459	150[c]	330
	1.294	0.844	0.56	9,900	17,700	...	0.764	0.459	200[d]	440
	1.295	0.844	0.56	18,400	32,800	5.5				
Perpendicular to test rods	1.298	0.844	0.56	18,600	33,300	6.4	0.764	0.459	200-225	460
	1.298	0.844	0.56	15,400	27,500	...	0.764	0.459	225-250	520
	1.299	0.844	0.56	16,000	28,500	4.9	0.764	0.459	250-275	570
	1.299	0.844	0.56	19,800	35,400	6.6				
Perpendicular to other two test directions	1.295	0.844	0.56	19,300	34,400	6.6	0.764	0.459	275	600
	1.295	0.844	0.56	18,400	32,800	7.1	0.764	0.459	175[e]	380
	1.294	0.844	0.56	18,700	33,400	5.8	0.764	0.459	225[f]	490
	1.295	0.845	0.56	19,000	33,900	5.4				

[a] Same rock rod not used in both tests.
[b] Sample failed after 10 sec.
[c] Sample failed after 20 sec.
[d] Sample failed after 3 sec.
[e] Sample failed after 20 sec.
[f] Sample failed after 50 sec.

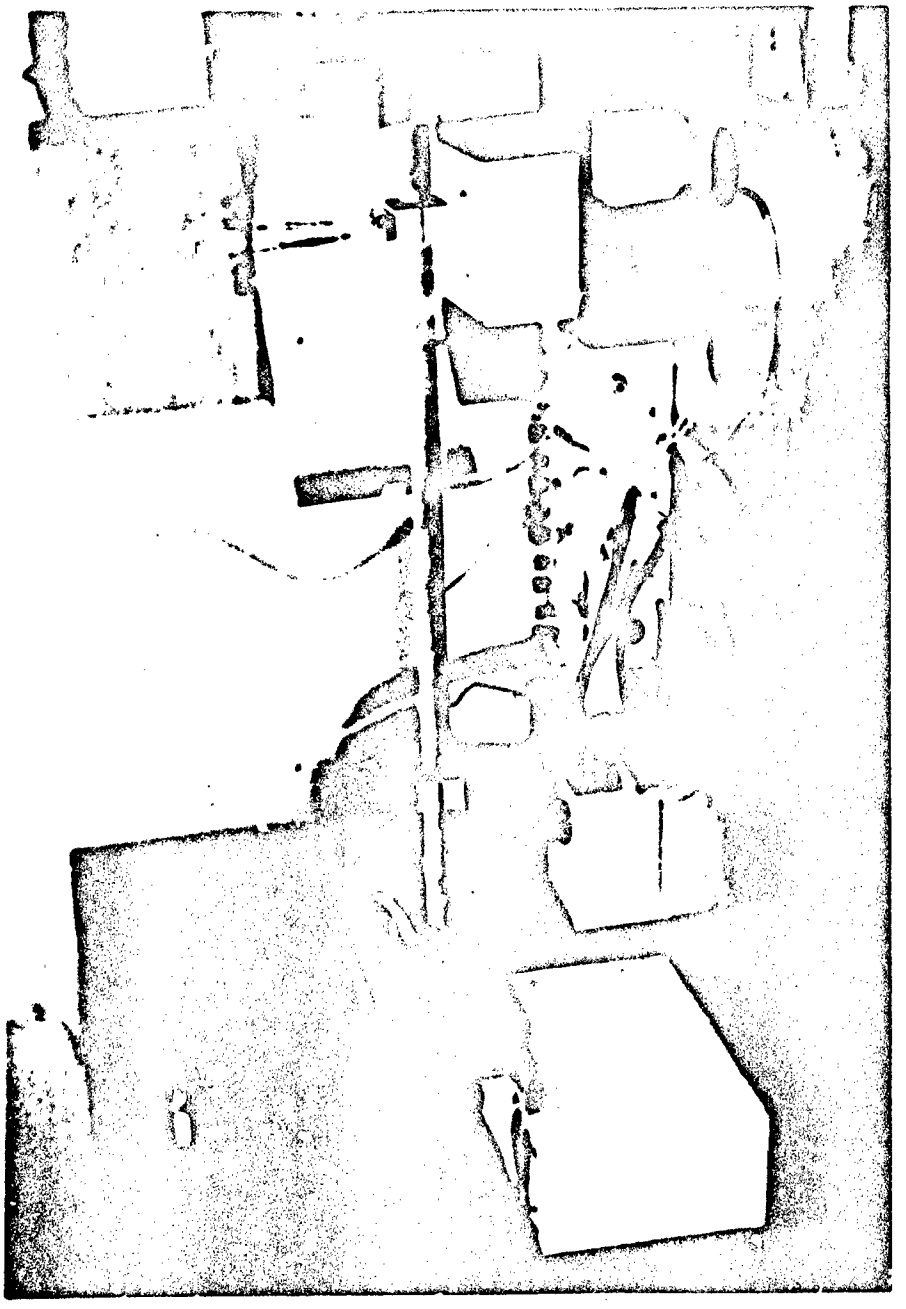

FIG. 10. Ballistic Arrangement for the Longitudinal Impact of Rock Rods.

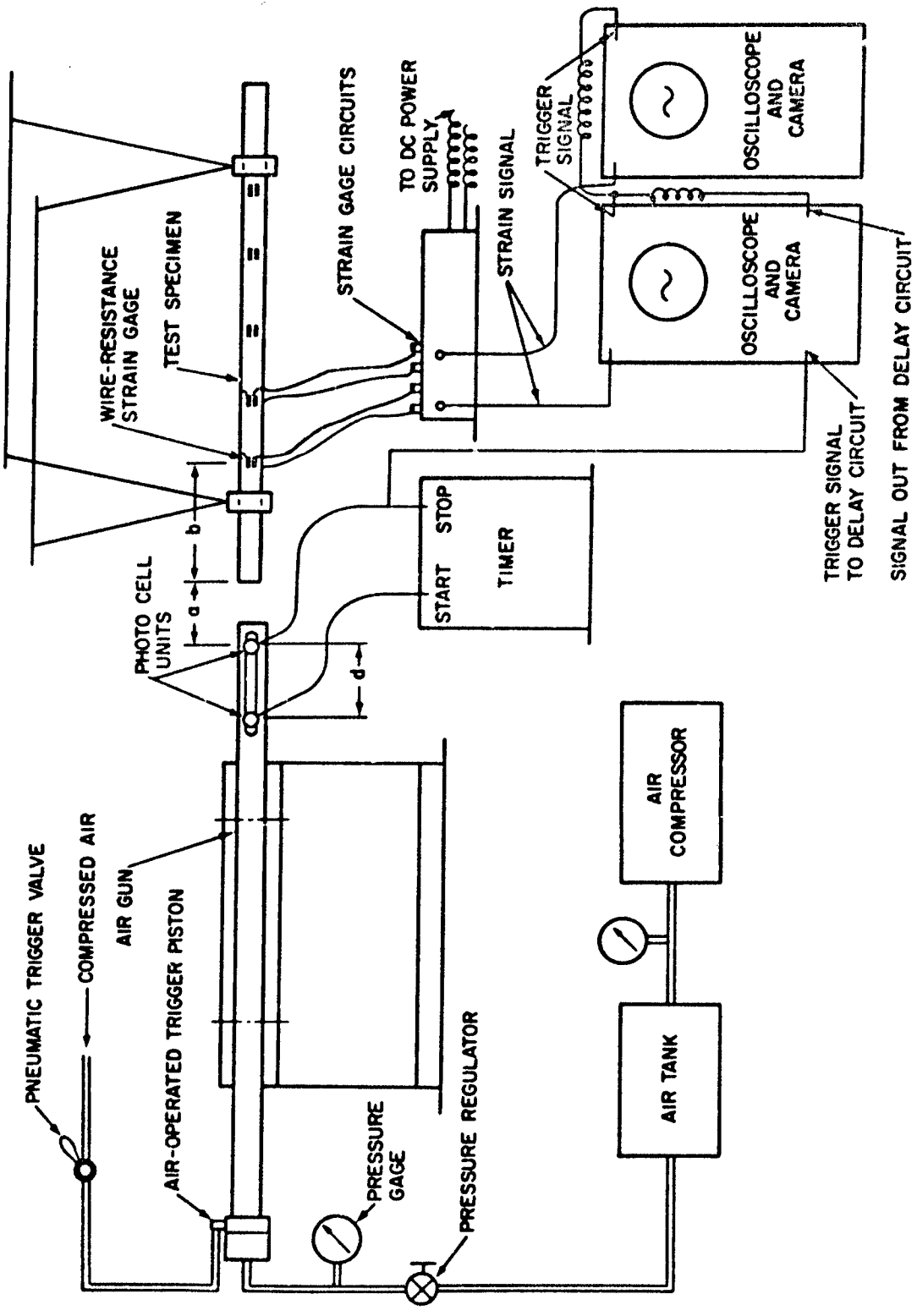

FIG. 11. Schematic of Experimental Setup.

and also to provide suitable light paths across the trajectory. The pulse from a second timing light was used to trigger the single sweep of all of the oscilloscopes simultaneously through a master delay circuit in one of the oscilloscopes. The delay time was adjusted so that all of the oscilloscopes were triggered just before the arrival of the pulse at the first strain-gage station on the test sample. The use of simultaneous triggering enabled the determination of the velocity of wave propagation from the arrival times of the first disturbance at each gage station.

Longitudinal strain pulses in the test rods were detected by 1/8-inch SR-4, FAP 12-12 foil-type strain gages in all but a few cases in which ¼-inch SR-4, FAP 50-12 foil gages were used. At each strain-gage station the gages were mounted in pairs in the longitudinal direction at the opposite ends of a diameter of the test rod. The gages were connected in series to eliminate any flexural wave component that might result from eccentricity of the projectile impact. The strain gages were mounted on the rods with Eastman 910 glue and in all cases, the strain gages were so located that their center lines were colinear in the longitudinal direction. A potentiometer circuit with a ballast resistor was used for all strain measurements. The applicability of strain gages for surface measurement of transients in nonmetallic rods had been demonstrated previously (Ref. 32).

Four observation stations were used in most tests to detect the change in the wave shape during transit. Two stations were used for samples when the effects of repeated shocks were of major interest, and as many as five and six stations were used in tests with protector caps on the sample rods, in tests using more than one gage size at a single section, and in tests using gages on an aluminum protector. The distance between two adjacent strain-gage stations was 3½ inches for the rock rods and 10½ inches for the aluminum rods. The maximum error in gage location was ± 1/64 inches. When two sets of strain gages were located at the same cross section, the additional pair of gages was rotated 90 degrees in position with respect to the regular gage pair.

During a test run, the strain signals were amplified, fed to the oscilloscopes, and photographically recorded. Each strain-time record was calibrated individually both before and after shooting. When the presence of permanent deformation was suspected under any gage, the base line of the strain-time record was checked by double exposing the film with a manually triggered sweep before terminal calibration.

The rebound velocity of the projectile in the aluminum-alloy-rod tests was obtained with a stroboscopic camera operating at an interframe time of 271.7 μsec. Attempts were also made to obtain the rebound velocity of the projectile for the spessartite rock rod tests with an intermediate speed framing camera, but it could not be operated slowly enough to cover more than a partial history of the impact process. The photographs obtained did show that the projectile was still traveling forward with an average velocity of 840 ips when half of the diameter of the

spherical projectile had already entered into the shadow of the rock fragments at the impact end of the test rod. In addition, the projectile frequently fell onto the test stand at a position indicative of a tendency to retain some component of its forward motion even subsequent to initial impact. Both of these observations suggest that there is no substantial rebound velocity of the projectile in the present tests.

The oscilloscope accuracy was estimated to be $\pm$ 2% and the gage factor accuracy, as claimed by the manufacturer, was $\pm$ 1%. Gage calibration was accomplished by the use of a known resistance that was connected in parallel with the foil resistance strain gages. The calibration principle is summarized as follows:

$$\frac{1}{R} = \frac{1}{R_c} + \frac{1}{R_g} \quad \text{or} \quad R = \frac{R_c R_g}{R_c + R_g} \tag{19}$$

$$\Delta R = R - R_g = \frac{-R_g^2}{(R_c + R_g)} \tag{20}$$

and the gage factor, $GF = (\frac{\Delta R}{R})/\epsilon$ (21)

where

R_g = resistance of the strain gage or gages at a certain measuring station

R_c = a known resistance

R = resultant resistance of R_g and R_c when both are connected in parallel

ΔR = increment of resistance

ϵ = strain

The calibration circuit is shown schematically in Fig. 12.

$$\text{Now strain } \epsilon = (\frac{1}{GF})(\frac{\Delta R}{R}) = (\frac{1}{GF})(\frac{\Delta R_g}{R_g}) = \frac{1}{GF}\,(\frac{-R_g}{R_c + R_g}) \tag{22}$$

and hence

$$\epsilon = (-\frac{1}{GF})/(1 + \frac{R_c}{R_g}) \tag{23}$$

Furthermore, the change in the voltage signal to the oscilloscope, ΔE, is proportional to the equivalent strain applied by using the shunt

resistance R_c, or $\epsilon = \gamma \Delta E$, where γ is a proportionality constant. Since ΔE is displayed on the oscilloscope screen as two parallel lines, the proportionality constant $\gamma = \epsilon / \Delta E$ can be readily obtained.

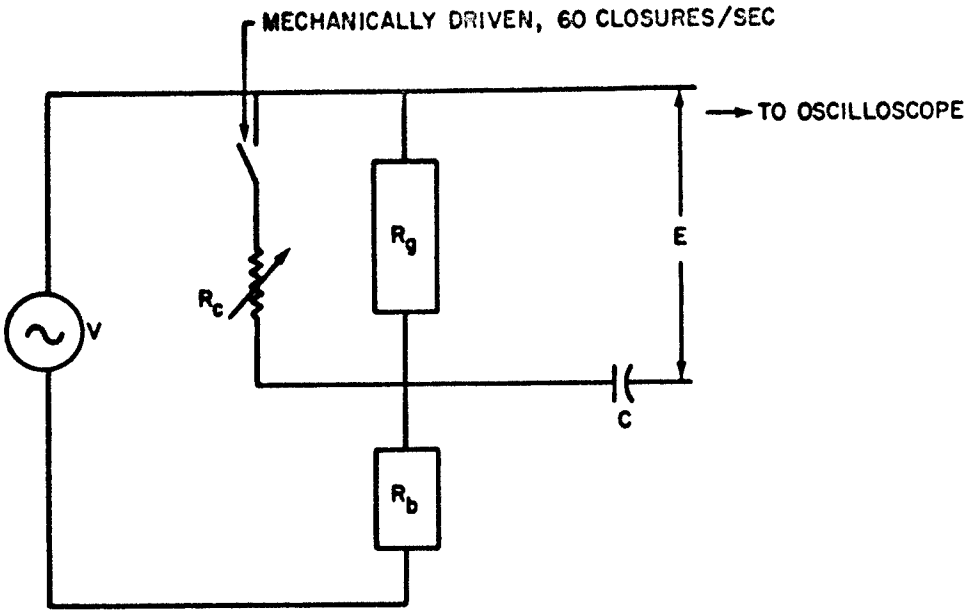

C = CAPACITOR, 0.1 mf
R_b = BALLAST RESISTOR, 120 Ω
R_c = CALIBRATION RESISTOR
E = SIGNAL
V = APPLIED VOLTAGE, ~24v
R_g = ACTIVE GAGES

FIG. 12. Strain Gage Calibration Circuit.

RESULTS AND DISCUSSION

Three different igneous rocks and an aluminum alloy were tested by means of the Hopkinson pressure bar technique. For completeness, diorite data from a previous investigation were included. Although not all shown, many repetitions of various tests were conducted to remove the inherent uncertainties of single observations for geologic materials that often have statistical properties on a macroscopic[1] basis. In such materials, even when carefully selected and prepared, apparent anomalies often

[1] Refers to dimensions that are large compared to interatomic distances, but small compared to the bar diameter and gage length.

represent nothing more than normal material variables. However, in the present case, such unexplained aberrations were virtually absent attesting to the high degree of uniformity of the samples.

ALUMINUM ALLOY

For the purpose of comparison with rock, several Hopkinson bar tests were performed on 2024 T-4 aluminum alloy that has been extensively studied under dynamic conditions (Ref. 33 and 34). A typical result is shown in Fig. 13. These runs were designed to determine experimentally the amount of geometrical dispersion in this metal of a pulse of similar shape and duration as produced in rock rods of identical diameter over the same distance of propagation. Aluminum was used because it is known to be virtually elastic below a well-defined stress level. A priori limits for the amount of this dispersion were calculated in the section on theoretical considerations. Another problem that must be considered with tests using strain gages is the validity of such surface measurements with respect to the average state of strain across the entire cross section of the test rod. This problem has been investigated theoretically by Davies (Ref. 16) and experimentally by Cunningham and Goldsmith (Ref. 33). For pulses of the type encountered in the present tests, their investigations indicate that the surface strain does not differ by more than 5% from the average strain in a macroscopically homogeneous material.

The highly complex and, at present, poorly understood fracture processes at the impact end of the rock rod prevent a prediction of the input pulse from a knowledge of the collision geometry, the mechanical properties of the projectile and target, and the initial projectile velocity. Consequently, the input to the rock rods must be accepted as the signal recorded at the first observation station. On the other hand, the transient produced in the aluminum rod can be approximated successfully on the basis of this same information plus a one-dimensional theory of elastic wave propagation in a bar (Ref. 34).

Figure 13 presents strain-time curves obtained from two strain-gage stations, G(1) and G(4) 10.5 inches apart. The observed change of momentum, calculated from the initial and the rebound velocities of the ¾-inch-diameter steel projectile, was 0.1815 lb-in. The impulse recorded by the first gage station was 0.178 lb-in., and the impulse recorded by the second gage station was 0.177 lb-in. Repeated testing showed essentially identical results.

The impulse was obtained by measuring the area under the initial positive portion of the force-time curve to the point of cross-over with the base line. The apparent error between the measured impulse and the change of momentum was less than 2% and corresponded to findings in a previous investigation (Ref. 34). The oscillations subsequent to the principal pulse are considered to be a manifestation of the dispersive

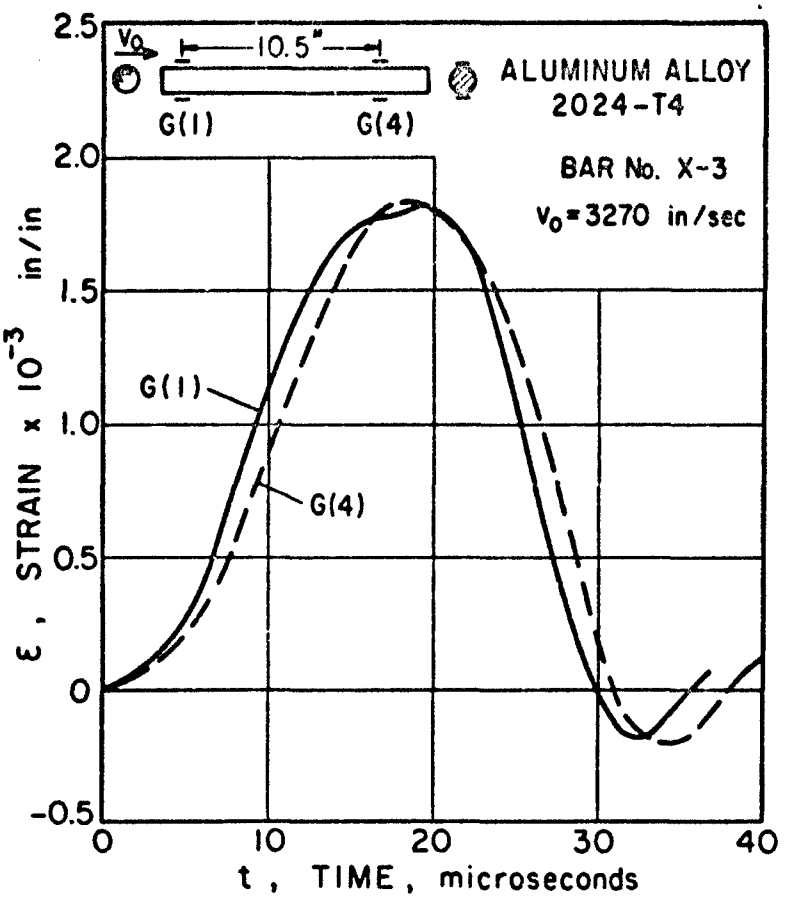

FIG. 13. Strain-Time Curves at Two Stations for a 2024-T4 Aluminum Bar 0.845 in. in Diameter Showing Results From the Impact of a Hard-Steel Spherical Projectile $\frac{1}{2}$ in. in Diameter. Observed change of momentum of the bullet: 0.1815 lb-in. Impulse recorded by gage (1): 0.178 lb-in. Impulse recorded by gage (2): 0.177 lb-in.

character of the test bar, due primarily to the effect of lateral inertia rather than to the three-dimensional character of the rod or internal friction, both of which would be manifested by successively larger pulse distortion with increasing distance of travel. This interpretation is largely substantiated by the fact that the reduction in magnitude in the impulse of the principal transient between the two gage stations does not exceed 2%, which is less than the experimental error for all runs. The increased amplitude of the tail at the second gage position does conform to the expected three-dimensional dispersive effect but quantitatively this characteristic can be neglected in the present investigations. Based on these considerations, the validity of the simple one-dimensional relation for a sufficiently accurate description of the propagation of the longitudinal pulses observed in both rock and metal rods of the size employed has been demonstrated. Furthermore, the characterization of the aluminum as an elastic material appears to be warranted.

The strain-time curves obtained from the aluminum tests were almost symmetrical about the maximum amplitude of the pulse, suggesting that the unloading process for these rods was almost the reverse of the loading process. No obvious attentuation or dispersion occurred between gage stations. The nearly identical pulses and wave velocities obtained for successive shocks on the same specimen provide evidence that previous shocks do not change the dynamic characteristics of this material. The results obtained for aluminum are in good agreement with those obtained in other studies on somewhat smaller diameter bars (Ref. 1 and 32) except for an observed slightly higher velocity of wave propagation in the larger bars.

ROCK RODS

Both virgin and shocked rock specimens were studied in this investigation. In most instances, repetitions of the various tests were performed to establish the reliability of the test results and to avoid or reduce the effects of possible statistical variations in the properties of the test samples selected. In the following discussion, the run number that appears in the test and figures describes simultaneously a particular specimen, identified by a capital letter, and the total number of impacts. Thus, H-5 means the fifth impact on test rod H.

The test results indicate that a higher projectile velocity does not necessarily induce a proportionally larger pulse in the instrumented portion of the rod. As a result of the fractures formed at the impact end of the rod such as those shown in Fig. 14, the theoretical equality between the observed change of momentum of the projectile and the recorded impulse, which was experimentally approximated in aluminum, is undoubtedly no longer valid for rock rods. In rock rods the impulse acquired by the fragments in the comminution zone, which is not measurable, is considerable. As an indication of this situation, the particles ejected from the

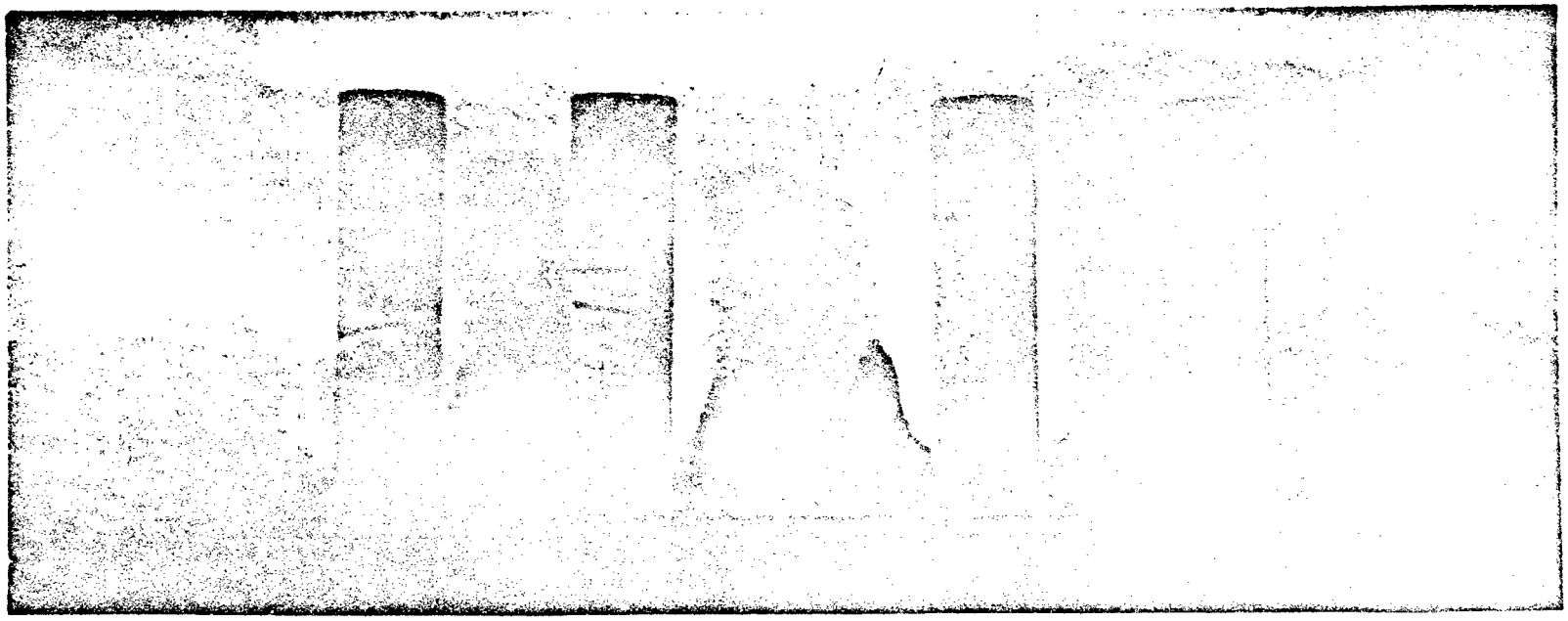

FIG. 14. Impact End Shear Fractures and Distal End Tensile Failures for Rock Cores Subjected to Longitudinal Impact Tests. The two cylinders at the left are of basalt, used as a wave trap glued on specimen J, and the two pyramids at the left were cut from the impact end after the tests after Runs J-2 and J-3. The two cylinders and pyramids at the right are of spessartite and were similarly obtained for Runs I-1 and I-2.

impact end of some spessartite rods traveled with a velocity sufficient to break an adjacent 3/16-inch-thick plastic safety shield.

Samples of the shocked rock previously subjected to longitudinal impact were tested to determine some of their static properties, and the results are presented in Tables 4–7. The letter designations used in these tables have the following meaning: the first letter indicates the specific rod, and the second letter denotes the relative sample position, starting with A at the distal end and adding letters in sequence toward the impact end.

BASALT. The strain-time curves for basalt are shown in Fig. 15 and 16. Two specimens of basalt with four strain gages each were successively shot three times each. These samples were designated as J and L and the results for sample J are shown in Fig. 15. The pulse shape produced in basalt is similar to that observed in spessartite, but has a longer duration, a greater tendency towards attenuation, and a larger amplitude for the same impact conditions.

An examination of the peaks of the strain-time curves at stations G(1) to G(4) in Fig. 15 shows an obvious general, albeit slight, attenuation as the wave progresses along the rod. This characteristic is occasionally obscured in the strain-gage signal from two adjacent stations because the low magnitude of the attenuation effect is counterbalanced or exceeded by experimental error and local effects due to minor sample inhomogeneities. Trial plots of the peak pulse amplitude in basalt as a function of travel distance show that the assumption of linear decay fits the observed data better than the assumption of exponential decay. The approximate expression for the one-dimensional pulse shape can be written as follows:

$$\epsilon = \epsilon_o (1 - \beta x) e^{i(pt - fx)} \qquad (24)$$

where

ϵ = strain, in/in

ϵ_o = peak amplitude of the strain-time curve at the first page, in/in

β = coefficient of linear attenuation, $in.^{-1}$

x = distance from the first gage along the bar, in.

p = natural frequency, rad/sec

t = time, sec

f = wave number, rad/in.

The average value for β was found to be 0.0160/in. for fresh material and 0.0083/in. for twice-shocked specimens. If the attenuation is assumed to be governed by exponential decay, use of the preceding notation would yield the relation

TABLE 4. Static Strengths of Shocked Basalt Cores[a]

Initial projectile velocity was 3,250 in/sec ± 1.5%.

Sample	Length, in.	Diam., in.	Cross sectional area, $in.^2$	Load at failure, lb	Compressive ultimate strength, psi	Young's modulus, psi x 10^{-6}	Tensile ultimate strength, psi
JD[b]	1.215	0.845	0.558	22,000	39,400	5.6	.....
JC[b]	.....	0.238	0.0445	50	.....	...	1,100
JB[c]	1.216	0.845	0.558	21,000	37,600	3.7	.....
JA[c]	.....	0.238	0.0445	37.5	.....	...	850
LD[b]	1.216	0.843	0.558	22,600	40,500	4.6	.....
LC[b]	.....	0.238	0.0445	62.5	.....	...	1,400
LB[c]	1.216	0.843	0.558	22,500	40,300	4.7	.....
LA[c]	.....	0.238	0.0445	62.5	.....	...	1,400

[a] Three previous shocks.
[b] Impact end.
[c] Distal end.

TABLE 5. Static Strengths of Shocked Spessartite Cores

Initial projectile velocity was 3,250 in/sec ± 1.5%.

Sample	Previous shocks, no.	Length, in.	Diam., in.	Cross sectional area, $in.^2$	Load at failure, lb	Compressive ultimate strength, psi	Young's modulus, psi x 10^{-6}	Tensile ultimate strength, psi
EE[a]	3	1.243	0.845	0.561	20,[illegible]0	37,200	2.3	.....
ED[a]	3	.....	0.238	0.0445	[illegible]25	.....	...	2,800
EC[b]	3	.....	0.238	0.0445	50	.....	...	1,100
EB[b]	3	1.244	0.845	0.561	31,400	56,000	2.5	.....
EA[b]	3	.....	0.238	0.0445	< 25	.....	...	< 600
BF[a]	3	1.244	0.845	0.561	32,700	58,300	3.4	.....
BE[a]	3	.....	0.238	0.0445	125	.....	...	2,800
BD[b]	3	.....	0.238	0.0445	100	.....	...	2,200
BC[b]	3	1.245	0.844	0.558	30,000	53,600	2.9	.....
BB[b]	3	.....	0.238	0.0445	75	.....	...	1,700
BA[b]	3	.....	0.238	0.0445	75	.....	...	1,700
FA	12	1.217	0.844	0.558	27,400	49,000	...	.....
FB	12	1.218	0.844	0.558	33,300	59,600	6.6	.....
FC	12	.....	0.238	0.0445	75	.....	...	1,700
FD	12	1.216	0.844	0.558	31,800	57,000	7.5	.....
HA	5	1.298	0.844	0.558	32,700	58,600	4.4	.....
HB	5	.....	0.238	0.0445	< 25	.....	...	< 600
HC	5	1.299	0.844	0.558	32,000	57,300	9.0	.....

[a] Impact end.
[b] Distal end.

TABLE 6. Static Strengths of Shocked Diorite Cores

Sample	Previous shocks, no.	Initial projectile velocity, in/sec[a]	Length, in.	Diam., in.	Cross sectional area, $in.^2$	Load at failure, lb	Breaking strength, psi
A-1	2	3,285, 3,300	1.0067	0.7659	0.461	12,500	27,115
A-2-2	1	3,285	1.0055	0.7660	0.461	13,000	28,200
B-1	1	3,300	1.2400	0.7613	0.455	13,000	28,571
C-1	2	3,300	1.2411	0.7633	0.458	8,000	17,467
D-1	2	3,300	1.2427	0.7626	0.457	9,450	20,678
D-2	2	3,300	1.2396	0.7616	0.456	9,600	21,053

[a] ½-in.-diameter steel sphere.

TABLE 7. Static Strengths of Shocked Leucogranite Cores[a]

Sample	Initial projectile velocity, in/sec	Length, in.	Diam., in.	Cross sectional area, $in.^2$	Load at failure, lb	Compressive ultimate strength, psi	Young's modulus, psi x 10^{-6}	Tensile ultimate strength, psi
NA	3,298,	.....	0.764	0.459	250[b]	.....	...	540
NB	3,310 and	1.295	0.844	0.560	11,300	20,200	...	...
NC	1,644	.....	0.764	0.459	≈ 213	.....	...	460
ND		1.294	0.844	0.560	18,200	32,500	...	...
OA	1,637,	1.294	0.844	0.560	13,400	23,900	3.4	...
OB	1,653 and	.....	0.764	0.459	150[c]	.....	...	330
OC	3,270	1.294	0.844	0.560	14,800	26,500	4.8	...
OD		.....	0.764	0.459	≈ 213	.....	...	460
OE		1.294	0.844	0.560	16,000	28,600	4.9	...
OF		.....	0.764	0.459	275[d]	.....	...	600
OG		1.294	0.844	0.560	16,300	29,100	3.8	...

[a] Three previous shocks.
[b] Sample failed after 20 seconds.
[c] Sample failed after 5 seconds.
[d] Sample failed after 5 seconds.

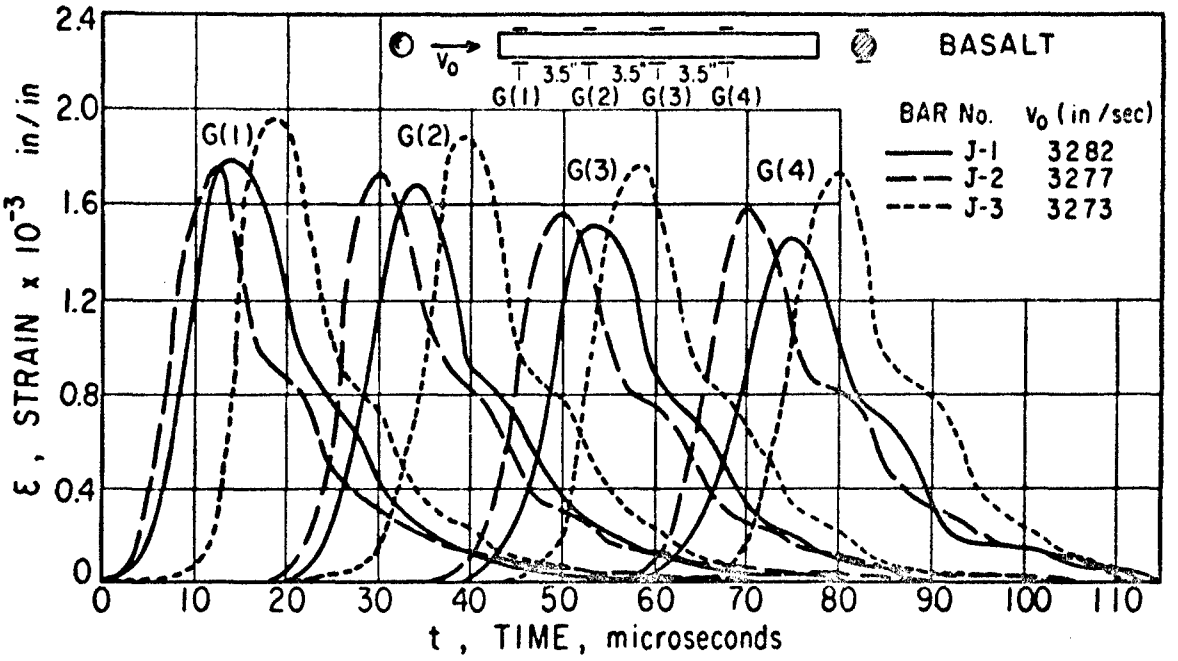

FIG. 15. Strain-Time Curves at Four Stations for a Basalt Bar 0.845 in. in Diameter Showing Results From the First, Second, and Third Impact of a Spherical Hard-Steel Projectile ½ in. in Diameter.

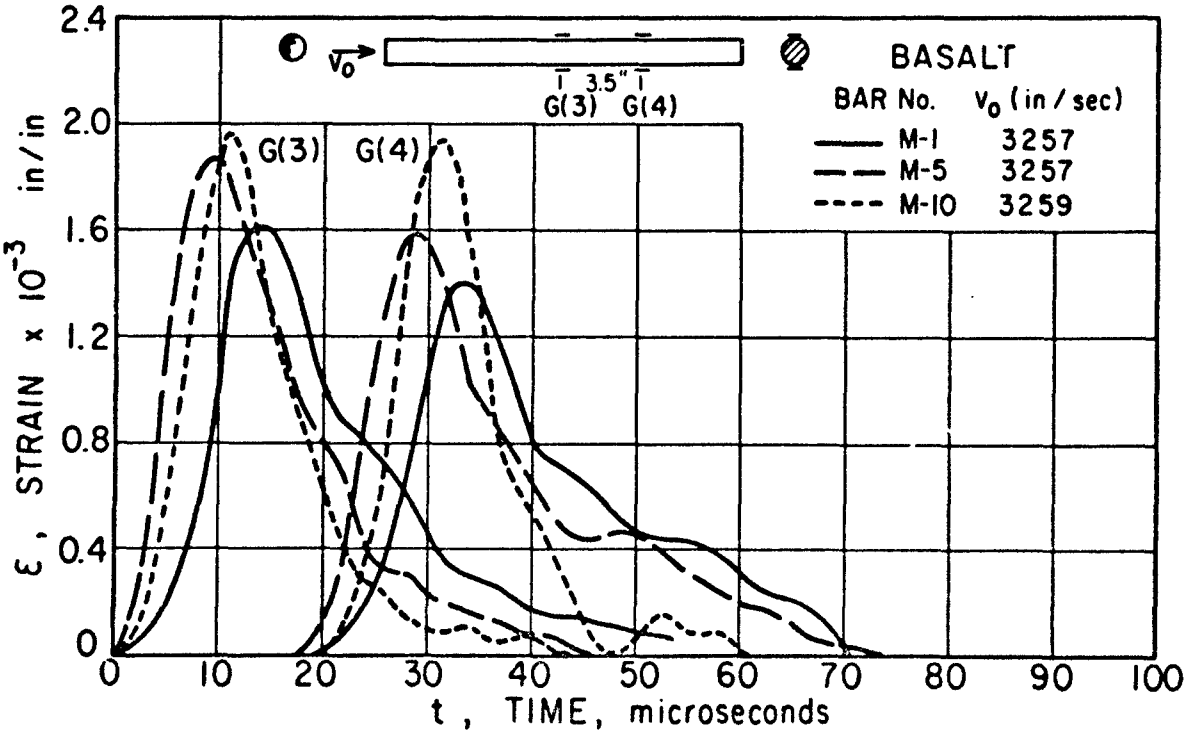

FIG. 16. Strain-Time Curves at Two Stations for a Basalt Bar 0.845 in. in Diameter Showing Results From the First, Fifth, and Tenth Impact of a Spherical Hard-Steel Projectile ½ in. in Diameter.

$$\epsilon = \epsilon_o e^{-\alpha x} e^{i(pt - fx)} \qquad (25)$$

where the optimum value of the attenuation coefficient α for all the data involving fresh specimens were found to be 0.012/in.

The static-test results for the shocked basalt are summarized in Table 4. Young's modulus for shocked basalt decreased from its original range of values of 5.8 to 7.2 x 10^6 psi to a new range in shocked material of 3.7 to 5.6 x 10^6 psi. The drop in Young's modulus is consistent with the increasing amplitude of the pulse for successive shocks on the same specimen, since the other conditions were left unchanged. The tensile and compressive strengths of the basalt exhibit no discernible change as a result of impact, when the fractured portions of the impact and distal areas of the rods are ignored. The present type of basalt exhibits a range of compressive strength from 31,800 to 41,200 psi and from 37,600 to 40,500 psi for virgin and shocked samples, respectively. The tensile strength for both was essentially the same.

Repeated shocks in basalt appear to have the following effects on the dynamic characteristics of the specimens: (1) a decrease in the coefficient of attenuation, and (2) an increase in the amplitude of the pulse. Specimen M was used to confirm these tendencies. Two strain-gage stations 3½ inches apart were subjected to ten successive impacts. The strain-time curves of the first, fifth, and tenth shocks are shown in Fig. 16 and are in good agreement with the predicted effects.

A previous investigation has indicated that porosity in rock is at least partially responsible for attenuation (Ref. 21). The test results achieved in this study using fresh basalt confirm this conclusion, but repeatedly shocked basalts behave differently. With repeated shocks, basalt shows a tendency toward decreasing pulse attenuation as shown in Fig. 16. Thus, with repetitive shocks of identical impulse, the mechanical damage produced within the rod beyond the zone of comminution reaches a saturation limit beyond which further damage does not occur. After this stage is reached, the basalt behaves like a new material with characteristics comparable to spessartite under the action of shocks with impulses no larger than that originally applied.

SPESSARTITE. The strain-time curves obtained from the dynamic tests with spessartite are shown in Fig. 17–19. The pulse shape produced in the spessartite is smooth and exhibits very little attenuation or dispersion. The pulse rise time is less than the time of decay. The unloading process shows a general tendency toward exponential decay, a feature that represents the largest single difference between the dynamic characteristics of the aluminum alloy on one hand and the spessartite and similar geologic materials on the other.

Test Runs H-1 to H-5, shown in Fig. 17 and 18, represent the results of five successive shocks on a single sample with five strain-gage observation stations. No significant variation could be found between

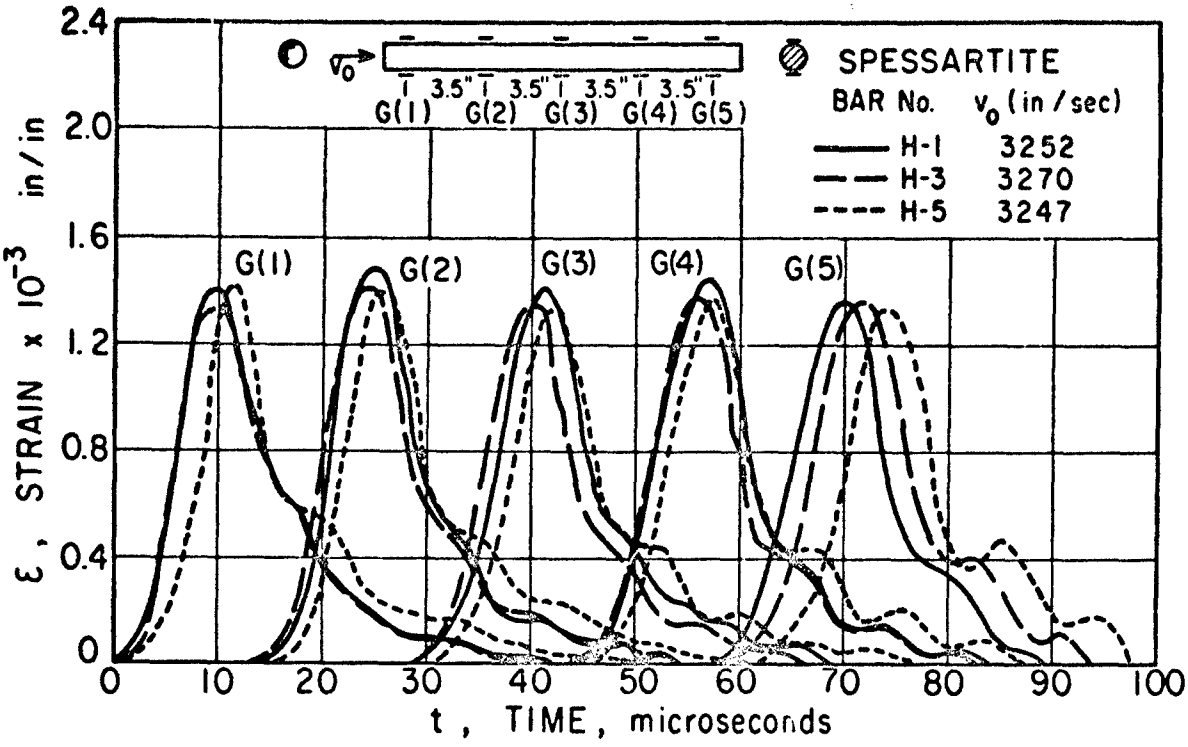

FIG. 17. Strain-Time Curves at Five Stations for a Spessartite Bar 0.845 in. in Diameter Showing Results From the First, Third, and Fifth Impact of a Spherical Hard-Steel Projectile $\frac{1}{2}$ in. in Diameter.

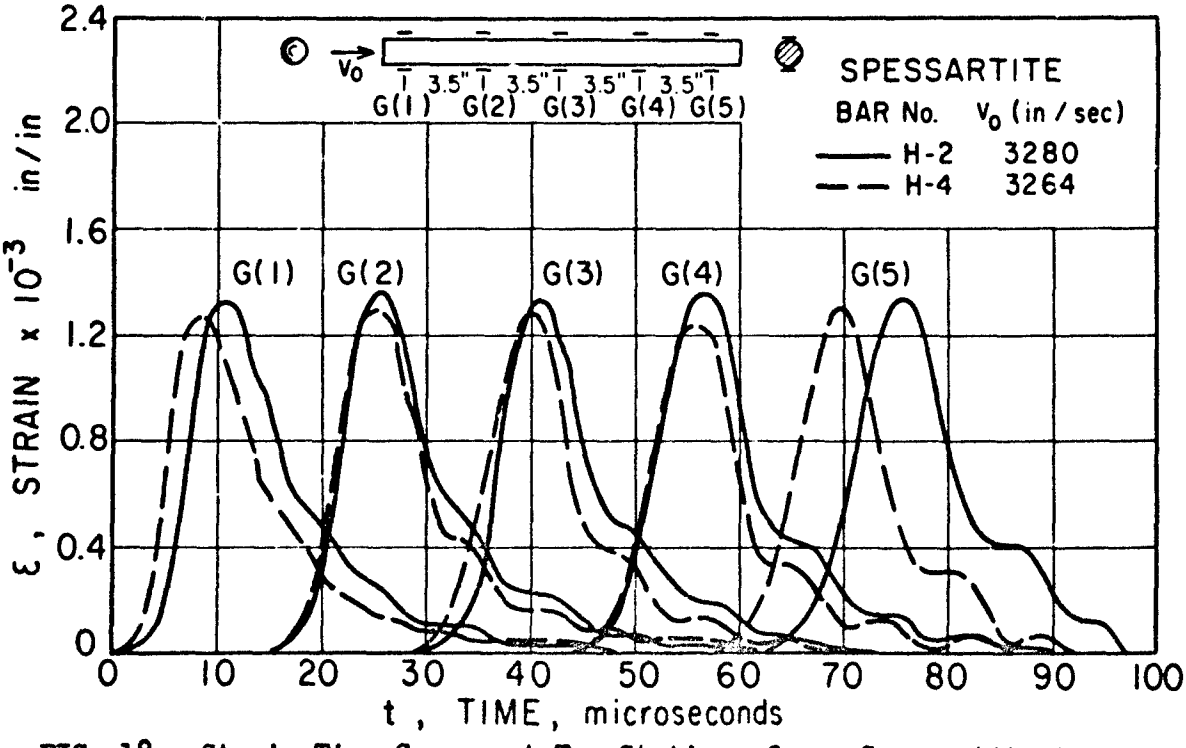

FIG. 18. Strain-Time Curves at Two Stations for a Spessartite Bar 0.845 in. in Diameter Showing Results From the Second and Fourth Impact of a Spherical Hard-Steel Projectile $\frac{1}{2}$ in. in Diameter.

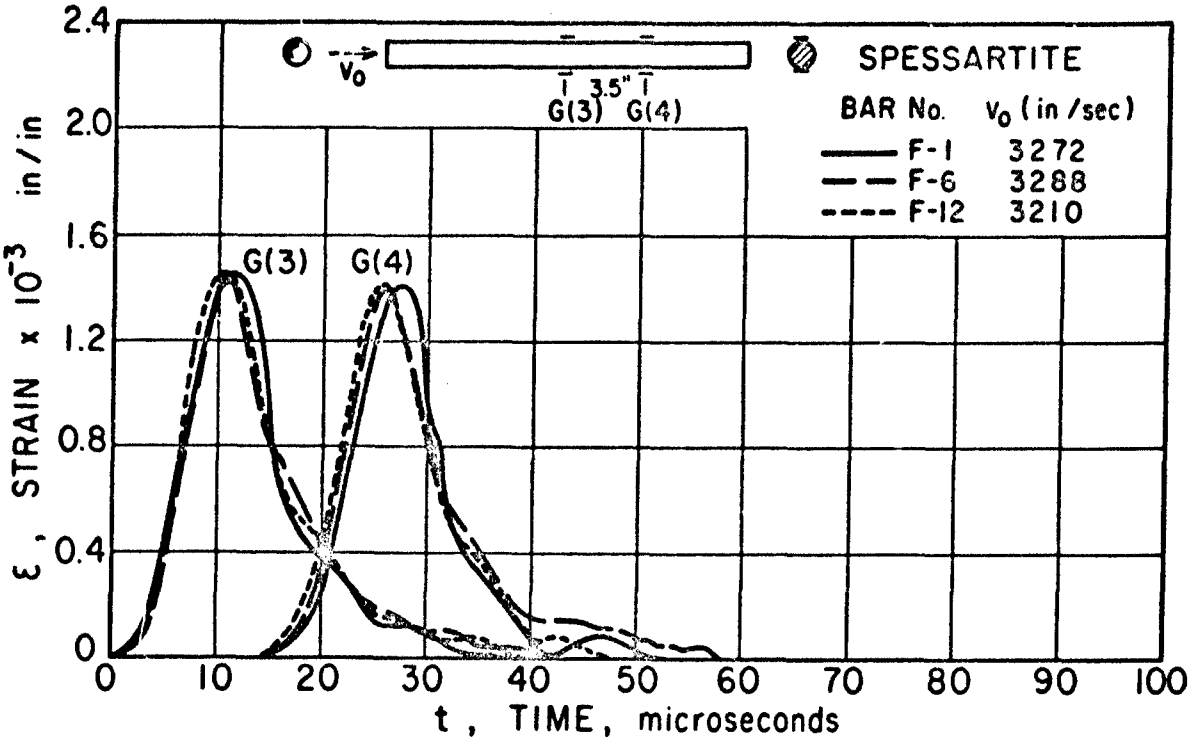

FIG. 19. Stress-Time Curves at Two Stations for a Spessartite Bar 0.845 in. in Diameter Showing Results From the First, Sixth, and Twelfth Impact of a Spherical Hard-Steel Projectile ½ in. in Diameter.

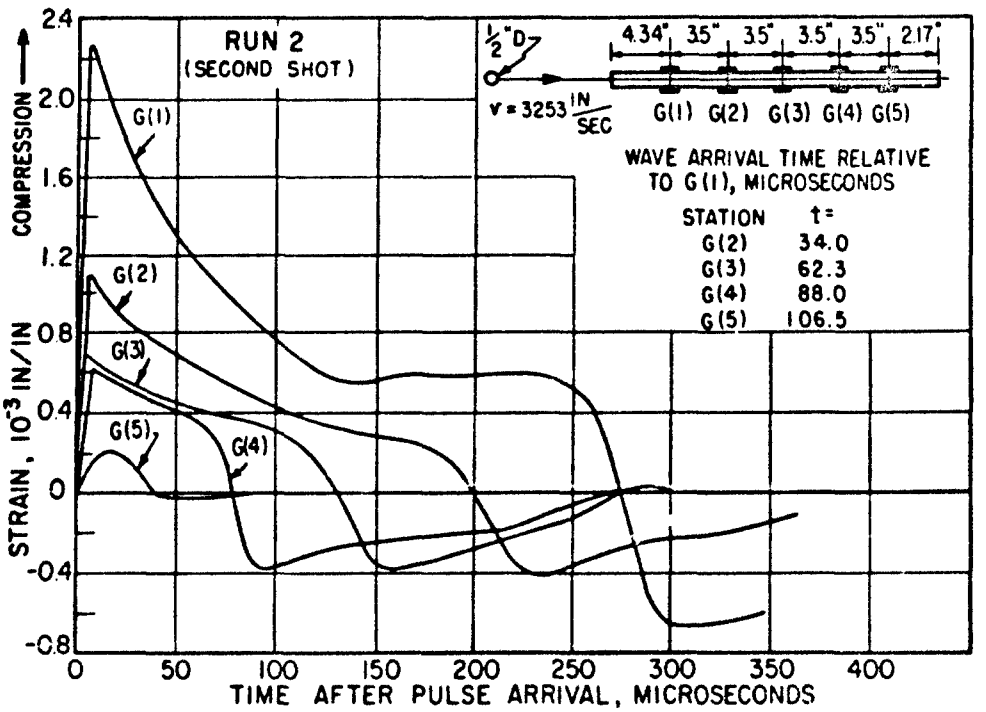

FIG. 20. Strain-Time Curves at Five Stations for a Diorite Bar 0.76 in. in Diameter Showing Results From the Second Impact of a Spherical Hard-Steel Projectile ½ in. in Diameter.

the results from these runs, which were conducted at an impact velocity of 3,260 ips. Repeated shocks under this loading condition had no influence upon pulse amplitude, shape, or wave velocity and hence, by inference, produced no shock-induced material behavior changes. Consequently, under the conditions employed the response of the spessartite was identical to that of aluminum alloy; both behaved as elastic materials exhibiting neither attenuation nor dispersion attributable to mechanical properties. Test Runs F-1, F-6, and F-12, shown in Fig. 19, subjected a single spessartite specimen to one, six, and twelve shocks, respectively, and confirm these general observations.

The static test results for shocked spessartite are summarized in Table 5. Rock rods B and E were subjected to three shocks each. Samples cut from these rods indicate damage to the Young's modulus but no significant damage to the compressive strength. Results from four samples show that Young's modulus in the shocked material has decreased from an average of approximately 9×10^6 psi to a value of only 3×10^6 psi. Samples taken near the impact point showed a loss of compressive strength, indicative of oriented fractures. Since the compressive strength of such rods as F, which were subjected to twelve shocks, remained unchanged, the spessartite closely simulates aluminum in its general behavior (except for brittleness) at the loading levels employed. In summary, spessartite can be regarded as an elastic material below its fracture point.

DIORITE. The results of experiments on diorite presented have been abstracted from a previous report (Ref. 1). Figures 20-22 show the pulse propagation in diorite rods. The marked attenuation of the wave without dispersion during the initial transit through the test rod is of particular interest. This behavior can be represented by a solid friction model such as that of Eq. 5 except that the attenuation of peak amplitude varied more nearly as $x^{-0.55}$ (x in inches) rather than as the exponential decay predicted by the mechanical model. The very sharp rise of the pulse followed by an exponential decay of the pulse in time at a given station resembles a true shock wave in form. Since this pulse will contain the entire spectrum of Fourier components, it should be extremely sensitive to any dispersive characteristics. The absence of such dispersion lends strong credence to the applicability of the solid friction model for the diorite tested.

Observations of the first pulse reflected from the distal end of the rod indicate that the amplitude of the reflected pulse, as recorded by the strain gages, increases with the return of the pulse toward the impact point. A plausible explanation for this phenomenon is to be found in the increasing damage produced by the first traverse of the pulse to the grain-to-grain bonds as the impact end is approached. This interpretation is corroborated by the drastic reduction in strain amplitude during initial transit that is indicative of large-scale energy absorption. Detailed microscopy of shocked diorite further supported this interpretation.

The static test results for shocked diorite are summarized in Table 6. Repeated impacts on the same test rod of diorite indicate the high degree of sensitivity of this rock to the passage of stress waves. With as little as two repeated impacts, using the same impulse as in other tests, a very dramatic reduction in both compressive strength and in Young's modulus could be observed in a shocked diorite. The consequence of this characteristic led to subsequent wave passage in a significantly different rock material from a mechanical viewpoint, when the same shock levels are used. Walsh, in a recent paper, shows that Young's modulus for an elastic solid containing cracks is less than that for an identical solid without cracks (Ref. 35). This is an excellent corroboration of the interpretation

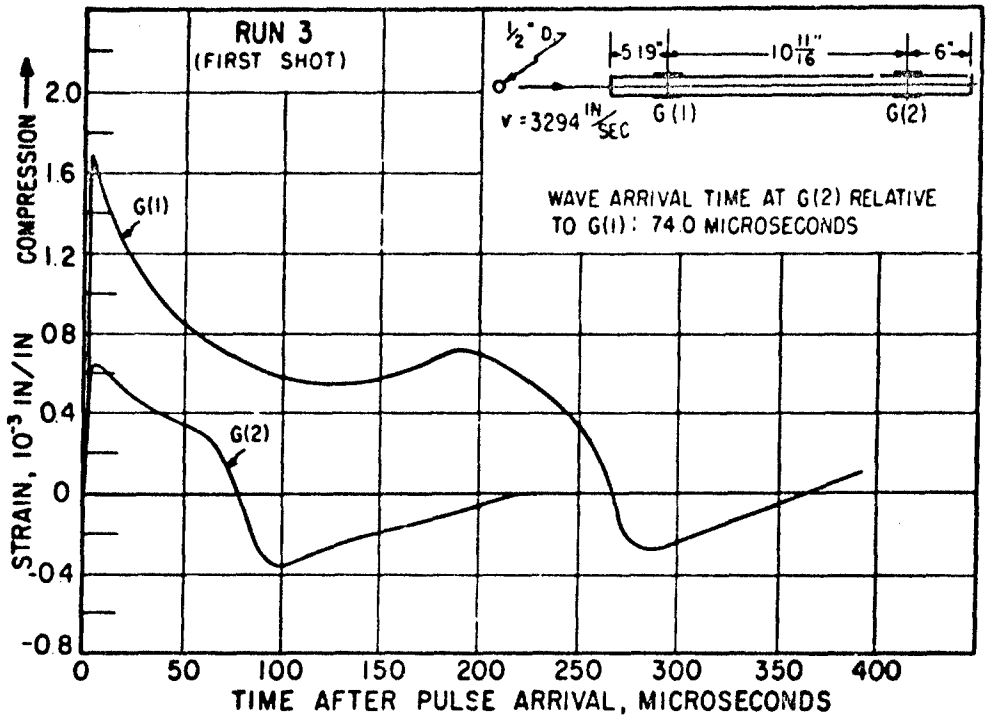

FIG. 21. Stress-Time Curves at Two Stations for a Diorite Bar 0.76 in. in Diameter Showing Results From the Impact of a Hard-Steel Spherical Projectile ½ in. in Diameter.

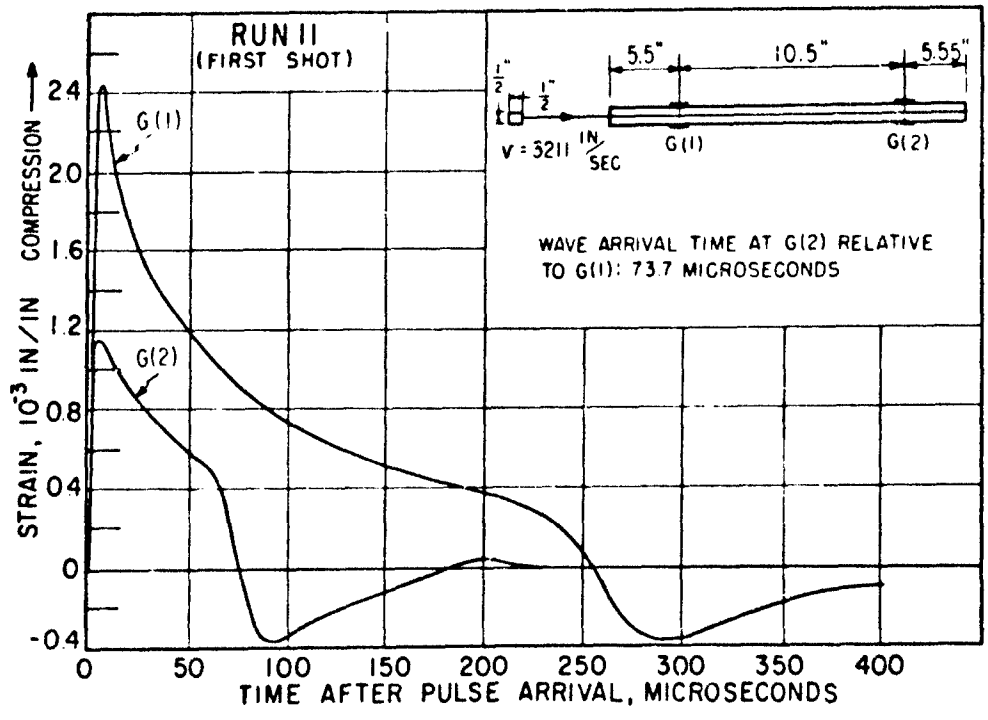

FIG. 22. Strain-Time Curves at Two Stations for a Diorite Bar 0.76 in. in Diameter Showing Results From the Impact of a Hard-Steel Flat-Nosed Projectile ½ in. in Diameter.

presented that relies upon grain-to-grain cracking and bond damage as the cause of lessened strength and modulus upon stress wave transit.

LEUCOGRANITE. Strain-time curves for leucogranite are shown in Fig. 23–29. The pulse characteristics for leucogranite are quite different from those of all other materials tested in this study. The drastic fluctuations in the rising part of the pulse and in the first portions of the decay part are believed to be due to reflections of the pulse at individual crystal boundaries. If these oscillations are disregarded, the rise of the principal portion of the pulse followed by an exponential decay is similar to the pulse observed in diorite. One point of difference between the leucogranite and all other materials tested was the presence of precursors, which precede the main pulse. This phenomenon in a homogeneous material is characteristic of a bending wave, but unlike bending wave behavior, increased distance along the test rods showed damping of the precursors. The existence of the precursors in this rock can be explained as the result of reflections from large grain boundaries.

The leucogranite used in these tests has a sufficiently coarse grain size so that the strain gages are comparable in length to individual mineral grains. The average grain size for diorite was 1½–2 mm but the average grain size for leucogranite was 5–6 mm. A 1/8-inch strain gage used on diorite will commonly cross two or three grains, but on leucogranite, the same gage will often be entirely located on a single crystal. Because of the possible importance of this problem, additional ½-inch-length strain gages were mounted at the first gage stations on test bars O, P, and Q, and in the tabulations these larger gages are denoted as G(1)*. This test sequence was designed to complement a previous investigation that had indicated that the pulse shape is not affected by the gage length provided the gage length is less than one-tenth the width of the pulse (Ref. 33). Although this study was performed in metals, the results are believed to be applicable to coarse-grained rocks as well. The strain-time curves G(1), obtained with 1/8-inch gages, and G(1)*, obtained with ½-inch gages were found to be very similar, as shown in Fig. 23–26. The one exception noted is illustrated in Fig. 29 where the longer strain gage detected a higher amplitude pulse, a result attributed to local variation in the test rod.

The pulse amplitude in the leucogranite attenuated significantly during transmission along the rod. The oscillations near the front of the pulse were damped out rapidly both along the pulse at a given station or for the pulse as a whole at successive stations, but the general shape of the principal portions of the pulse remained almost undispersed. The sharp decrease shown for the pulse durations at G(2), G(3), and G(4) in Fig. 26 and 29 are due to the cancellation of the incident pulse by parts of the reflected wave. This decrease is not due to dispersion, as can be confirmed by the fact that the time corresponding to the cross-over point of the strain-time curves and the base line decreased gradually from the first to the last gage station, as shown in Fig. 26 and 28.

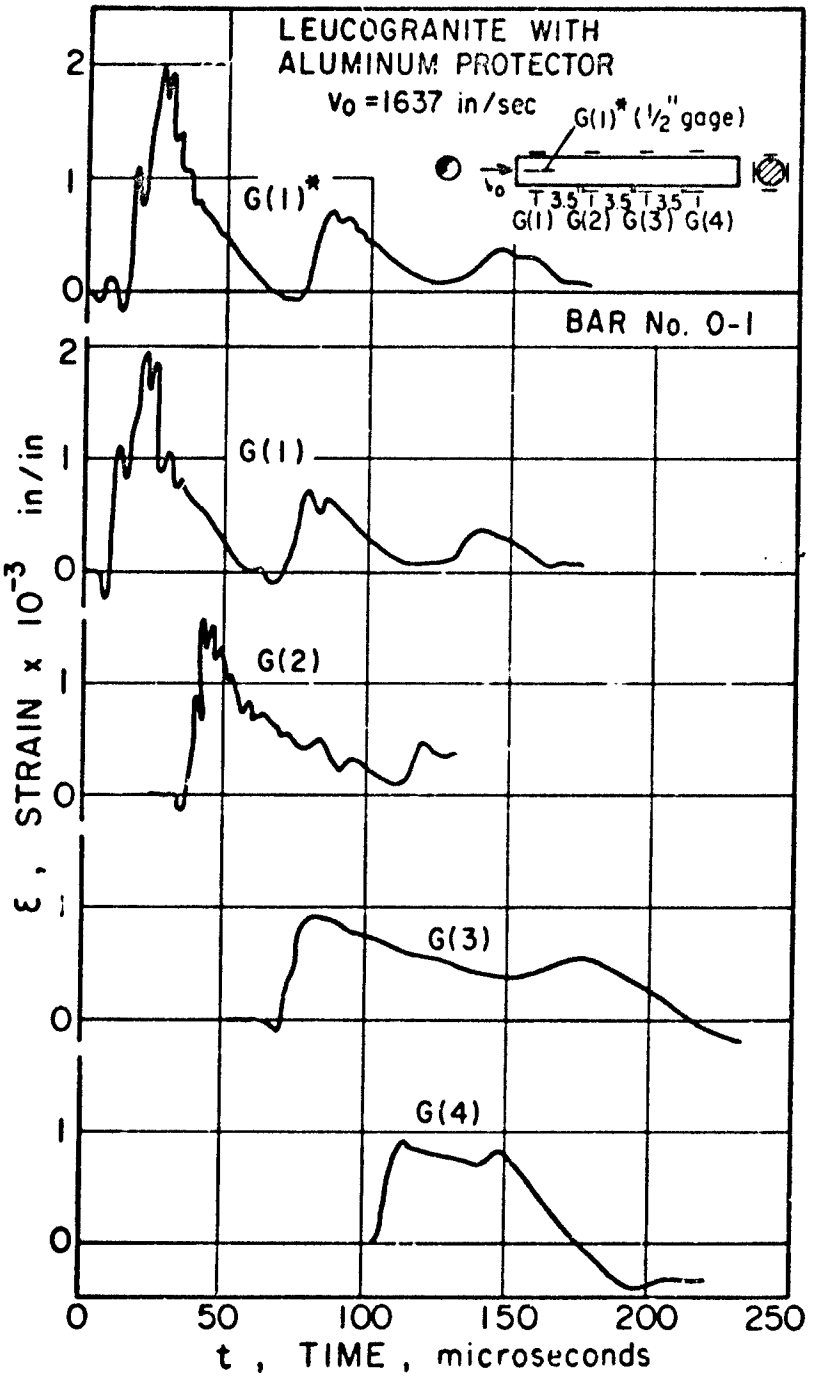

FIG. 23. Strain-Time Curves at Four Stations for a Leucogranite Bar 0.845 in. in Diameter Showing Results From the Impact of a Hard-Steel Spherical Projectile ½ in. in Diameter.

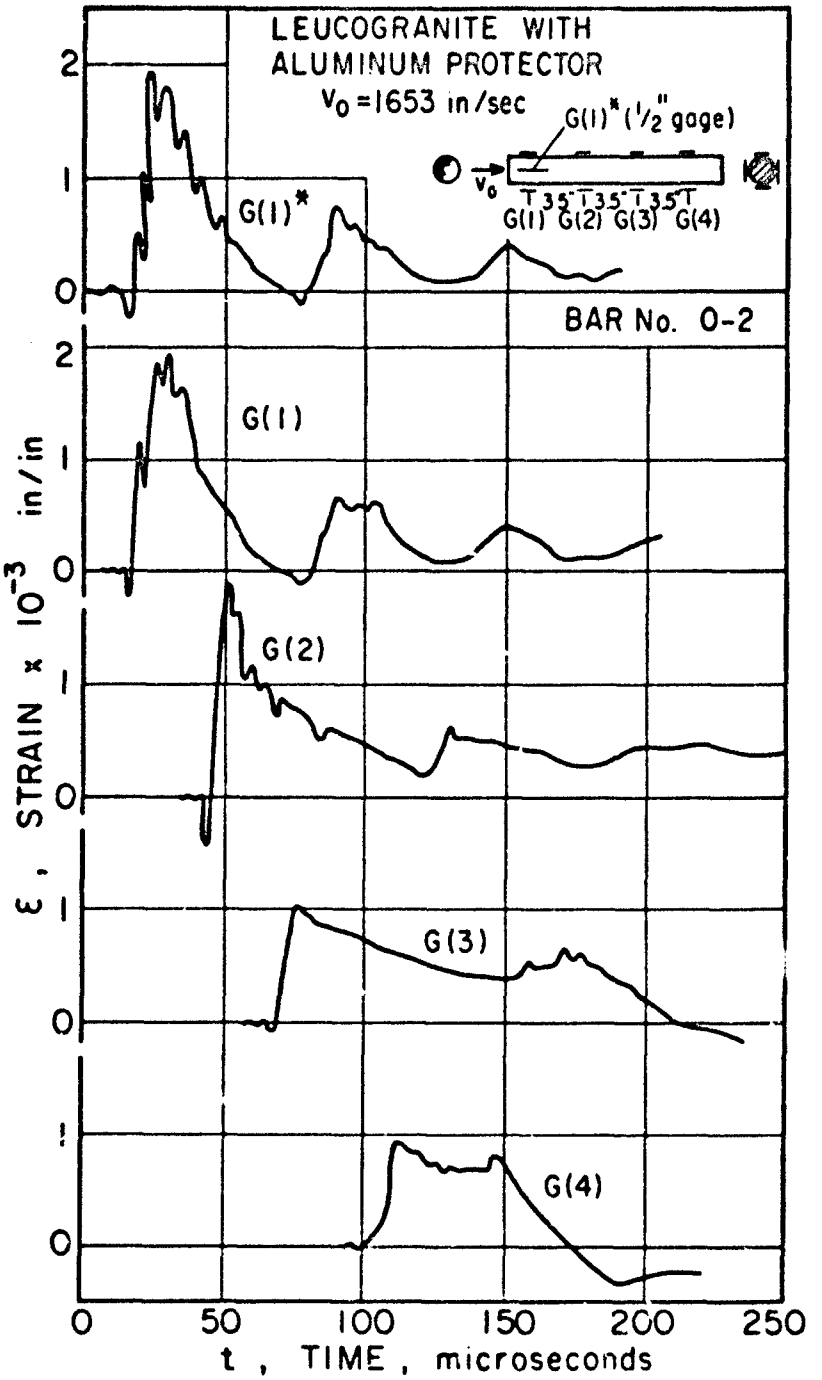

FIG. 24. Strain-Time Curves at Four Stations for a Leucogranite Bar 0.845 in. in Diameter Showing Results From the Second Impact of a Hard-Steel Spherical Projectile ½ in. in Diameter.

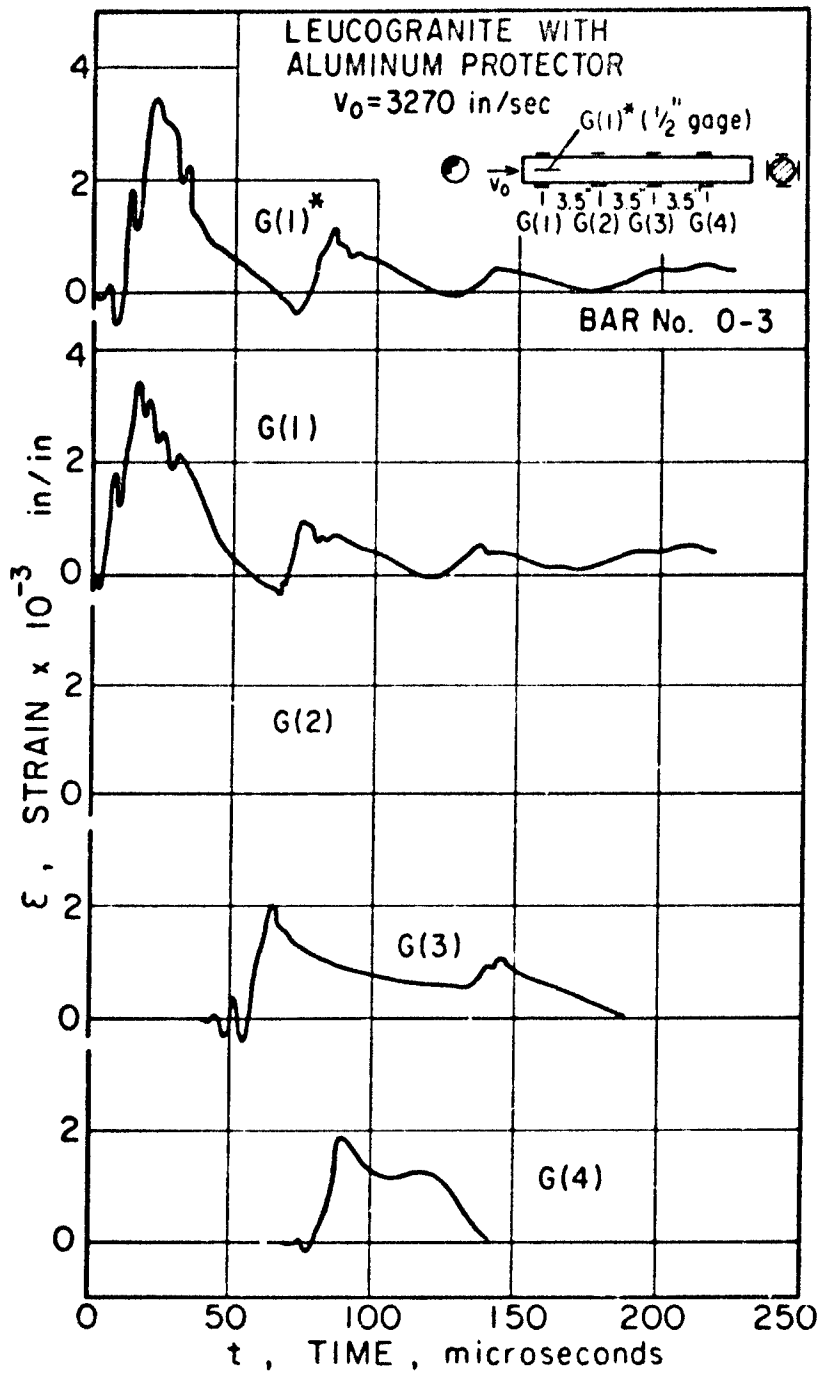

FIG. 25. Strain-Time Curves at Three Stations for a Leucogranite Bar 0.845 in. in Diameter Showing Results From the Third Impact of a Hard-Steel Spherical Projectile ½ in. in Diameter.

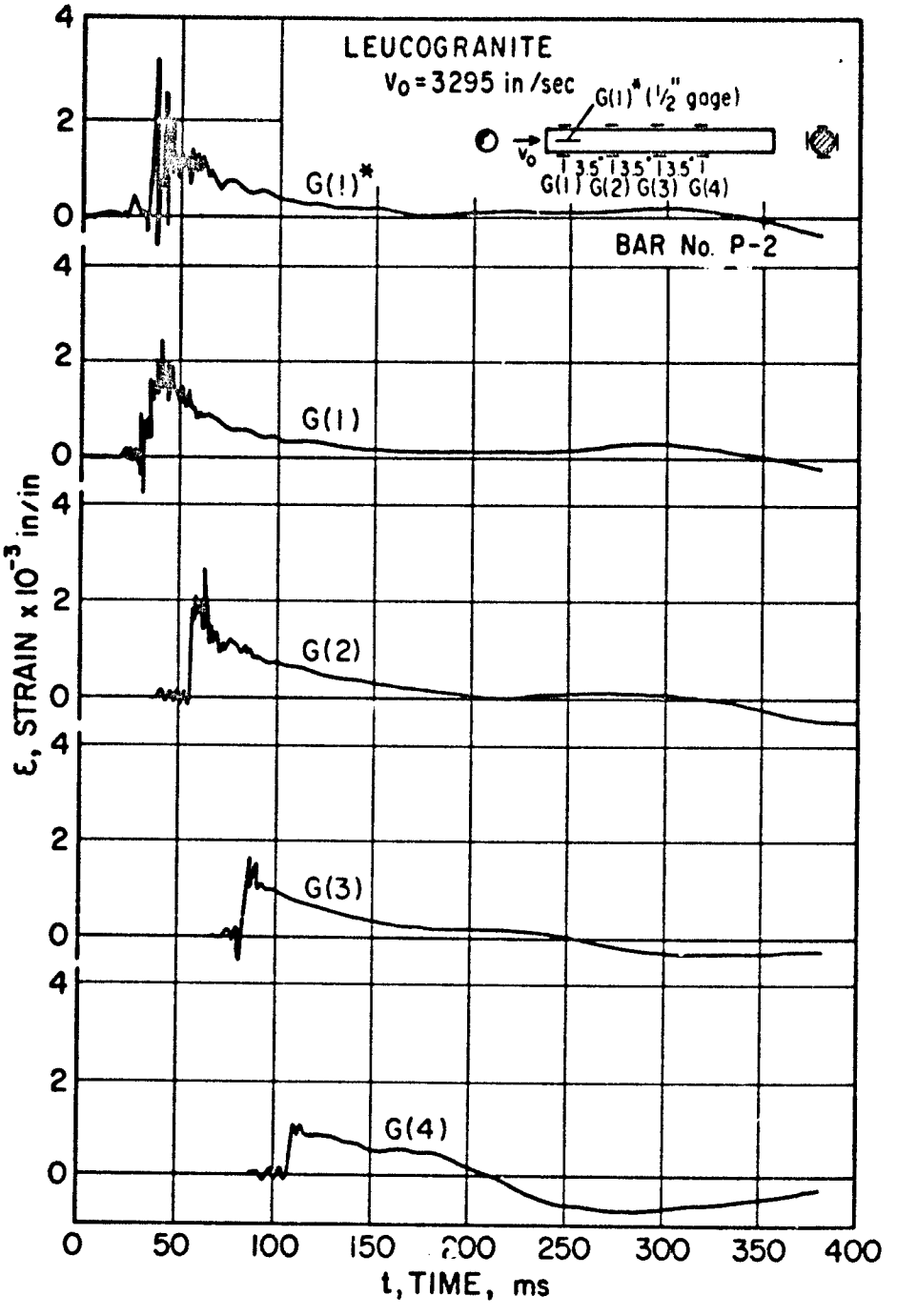

FIG. 26. Strain-Time Curves at Four Stations for a Leucogranite Bar 0.845 in. in Diameter Showing Results From the Second Impact of a Hard-Steel Spherical Projectile ½ in. in Diameter.

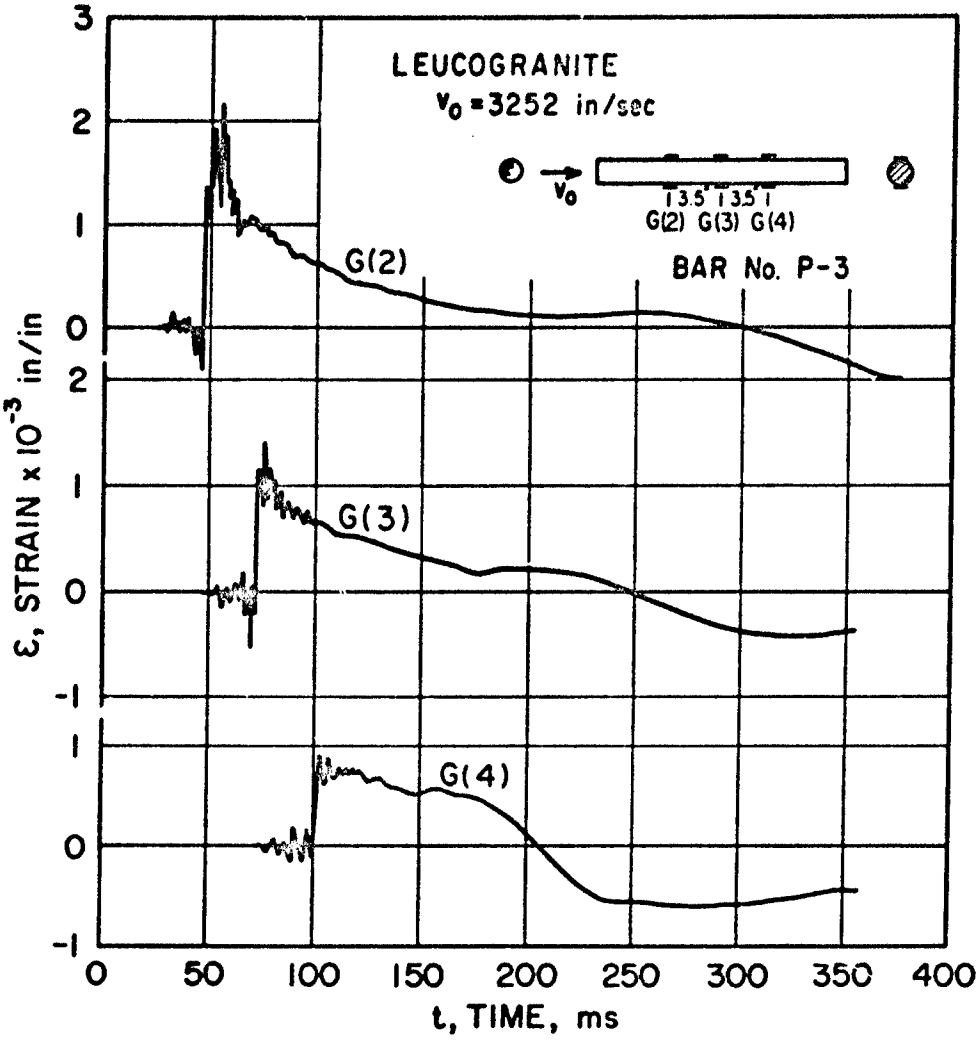

FIG. 27. Strain-Time Curves at Three Stations for a Leucogranite Bar 0.845 in. in Diameter Showing Results From the Third Impact of a Hard-Steel Spherical Projectile ½ in. in Diameter.

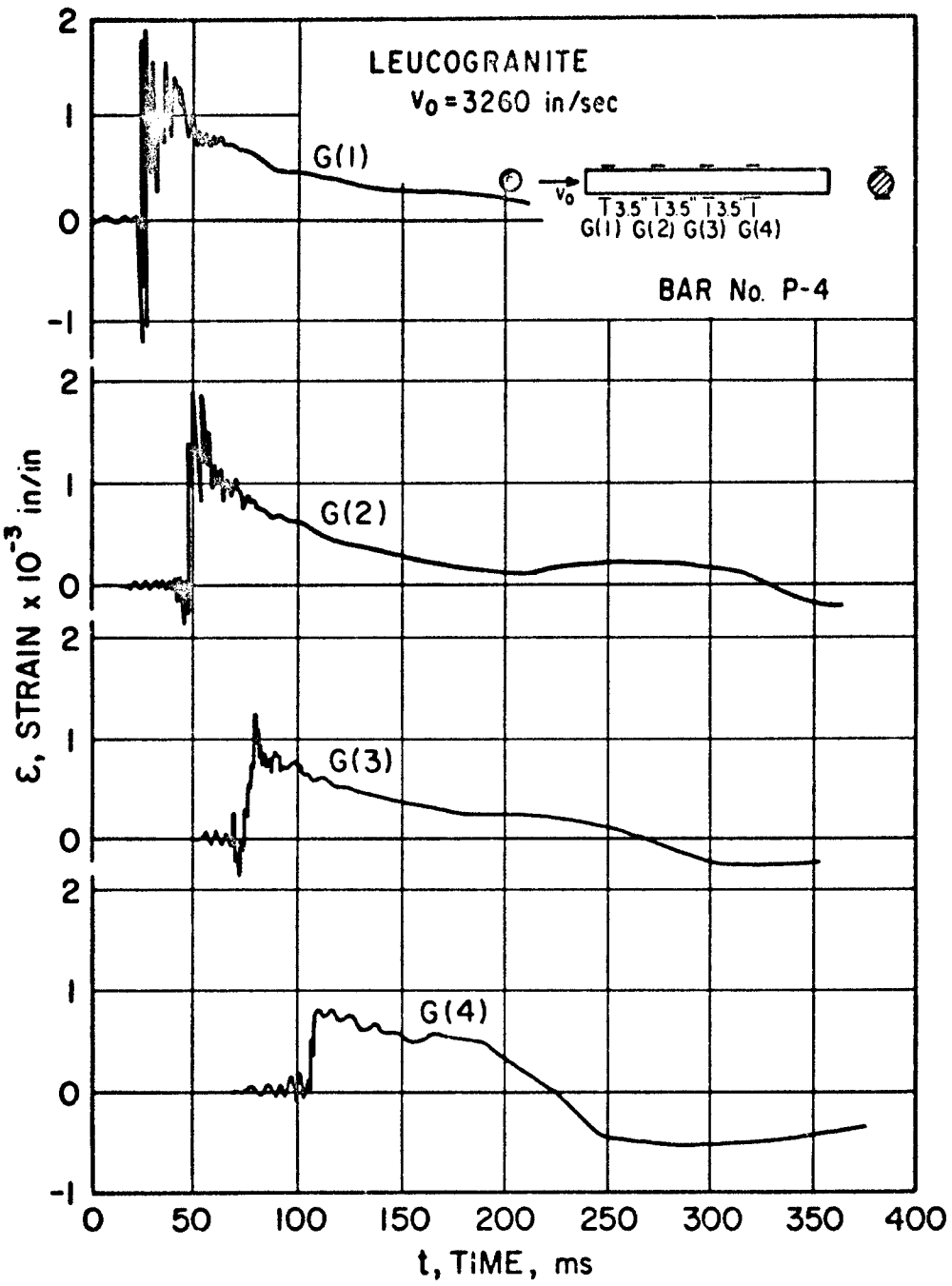

FIG. 28. Strain-Time Curves at Four Stations for a Leucogranite Bar 0.845 in. in Diameter Showing Results From the Third Impact of a Hard-Steel Spherical Projectile ½ in. in Diameter.

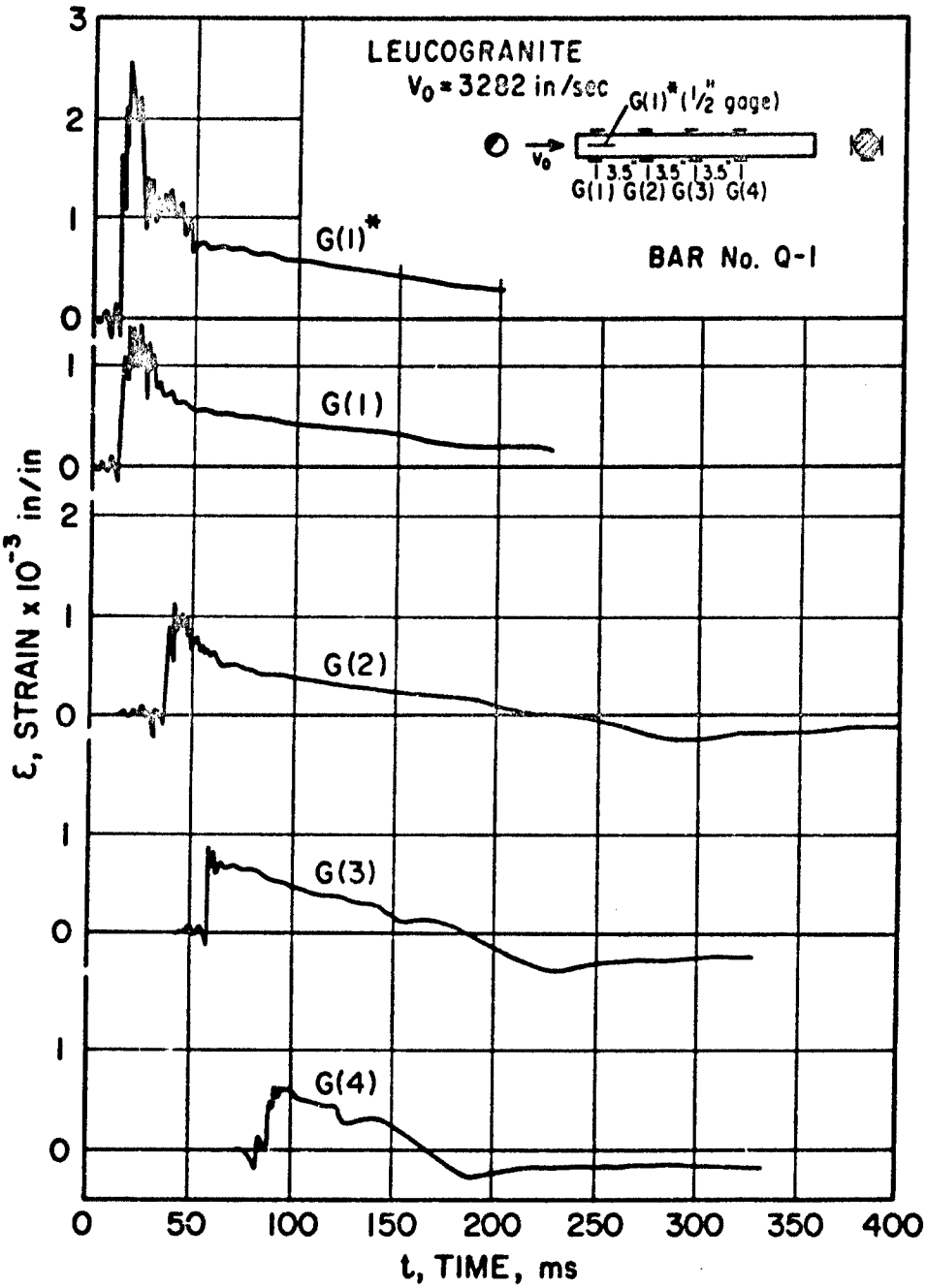

FIG. 29. Strain-Time Curves at Four Stations for a Leucogranite Bar 0.845 in. in Diameter Showing Results From the Impact of a Hard-Steel Spherical Projectile ½ in. in Diameter.

The use of longer strain gages did not reduce the drastic fluctuations of the strain-gage signal from the leucogranite. Probable causes for these oscillations are the weaker grain bonds and the large cleavage surfaces present in the leucogranite. Furthermore, the vibrations of the individual grains were apparently of sufficiently low frequency to be readily detected by the equipment in use.

The lower over-all bond strength of the leucogranite relative to the other rock types tested is evidenced by the noticeable friability of the rods during diamond sawing, even in fresh material, and by the inability of the impact end fragments to remain as large coherent pieces following impact. A lower bonding strength, as present in the leucogranite, provides both less constraint to the motion of individual grains as crystals, and less damping for the oscillations of a single crystal.

An interesting aspect is that although leucogranite is the weakest rock tested statically, the reflected tensile pulse in the test rods would consistently break the stronger materials at the distal end as shown in Fig. 14, but the leucogranite rod usually survived intact in this zone. A comparison of respective pulse shapes provides a partial explanation, as the extra long pulse duration and the drastic attenuation in the leucogranite both lead to a comparatively smaller amplitude of the net reflected tensile pulse. As long as this reduced pulse does not exceed the dynamic tensile strength of the rod, the rod will not break. Similar rock behavior has been noted in studies of explosively induced fractures in rock.[1]

The action of the spherical projectile, used in these studies and at the velocities employed, would always fragment the impact end of the rock rods. To generate pulses in rock rods without such fractures, aluminum protectors were employed at the point of collision. The results of such a test are shown for specimen O in Fig. 30. The strain-time curves for leucogranite studied as the O series of tests are shown in Fig. 23–25 and differ from the results of the P and Q series in Fig. 26–29 (which did not include the protective device) by showing repeated periodic rises in the decaying portion of the pulse instead of steady decay. This phenomenon is due to interfacial reflections from the protector-rock-rod interface, which causes second compressive loadings of the leucogranite. A numerical substantiation of this observation has been carried out.

The initial velocity of the projectile for test Runs O-1 and O-2 was reduced to one half the usual velocity for the tests conducted on all other samples. In comparing the strain-time curves of Fig. 23 and 24 with the corresponding curves of Fig. 26–29, the results show that in the peak

[1] Austin, C. F., J. K. Pringle, and S. A. Finnegan. "The Fracture and Breakup of Rock," a paper presented at the 1965 Annual Meeting of AIME.

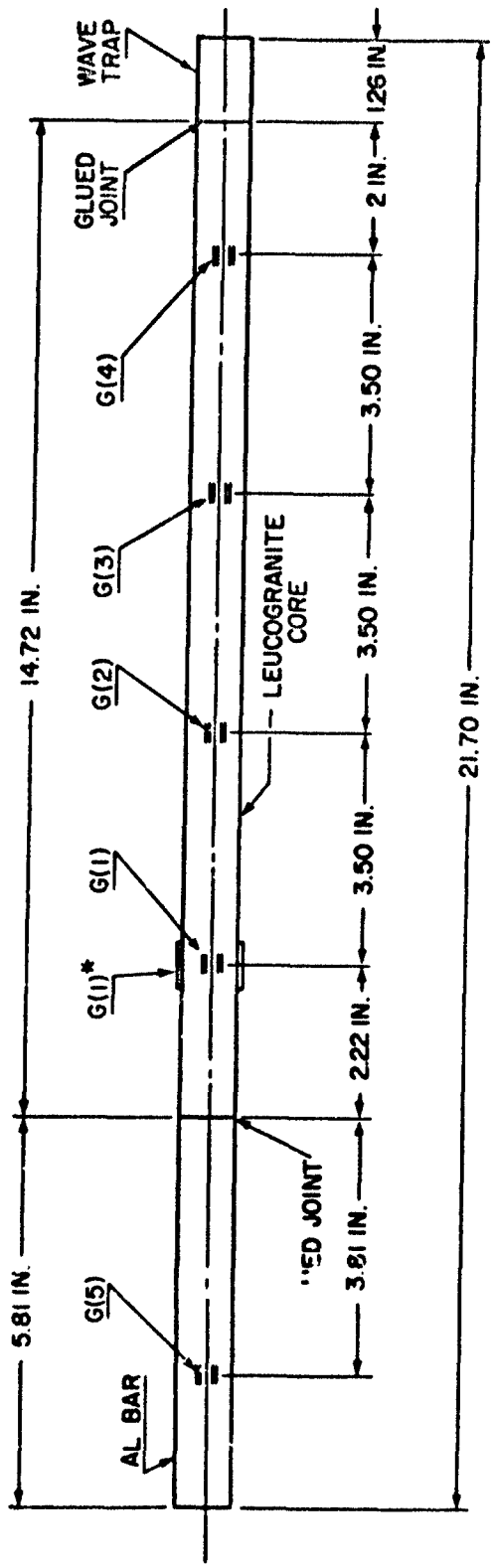

FIG. 30. Test Specimen for Run O-1, Leucogranite with Aluminum Protector.
Strain gage used for station G(1)*, SR-4 Type FA 50-12 (1/2" gage length).
For other stations, SR-4 Type FAP 12-12 (1/8" gage length). Glue used:
Eastman No. 910.

amplitudes obtained from the decreased velocity tests were proportionally much higher than those obtained from tests with the higher normal test velocity but without the aluminum protector cap. The peak amplitudes of G(1) for Runs 0-1 and 0-2, both at lowered impact velocity, are in the range of 1.94 to 2.00 x 10^{-3} in/in, while for the P and Q series with the higher impact velocity but no aluminum protector, the corresponding amplitudes are in the range of 2 to 3 x 10^{-3} in/in. The input pulses observed in the aluminum are smooth, as shown in Fig. 31 for Runs 0-1, 0-2, and 0-3.

The preceding phenomena are explained by a number of factors:

1. The projectile will rebound with a larger velocity from an aluminum surface than from a rock surface, resulting in a larger change of momentum for the same mass and initial projectile velocity.

2. No fragmentation occurs anywhere if the projectile strikes the aluminum protector instead of hitting the rock rod, permitting the transmission of more energy into the rock section of the test rod and avoiding energy absorption in comminution.

3. Shorter impact times and pulse durations result with the aluminum protector, requiring higher amplitudes for the same impulse.

A comparison of wave shapes in the leucogranite impacted both with and without an aluminum protector shows that the stress wave in the leucogranite assumes a similar form in both cases. This observation indicates that the fracture of the unprotected end of a rock rod is not the principal determinant of the wave shape in the rock rod, and that the rock rod itself will transform the smooth input pulse shown in Fig. 30 into a pulse exhibiting significant high-frequency fluctuations.

Run 0-3 is a repeated test with an aluminum protector at the standard initial velocity of the projectile. The corresponding pulse amplitudes obtained from Run 0-3 are about 25–50% higher than those obtained from the P series. The strain-time curves for Run 0-3 are shown in Fig. 25.

An examination of the peak amplitudes of the strain-time curves at stations G(1) to G(4) in Fig. 26–29 clearly reveals a tendency toward pulse attenuation with distance along the rock rod. Semilogarithmic plots of the peak amplitude as a function of distance indicate that the assumption of exponential decay provides a reasonable fit for the data at hand. The coefficient of attenuation was found to be approximately $\alpha = 0.072$, so that the propagation of the pulse in the leucogranite can be expressed by:

$$\epsilon = \epsilon_o e^{-0.072x} e^{i(wt - kx)} \qquad (26)$$

The attenuating tendency of the leucogranite is considerably higher than

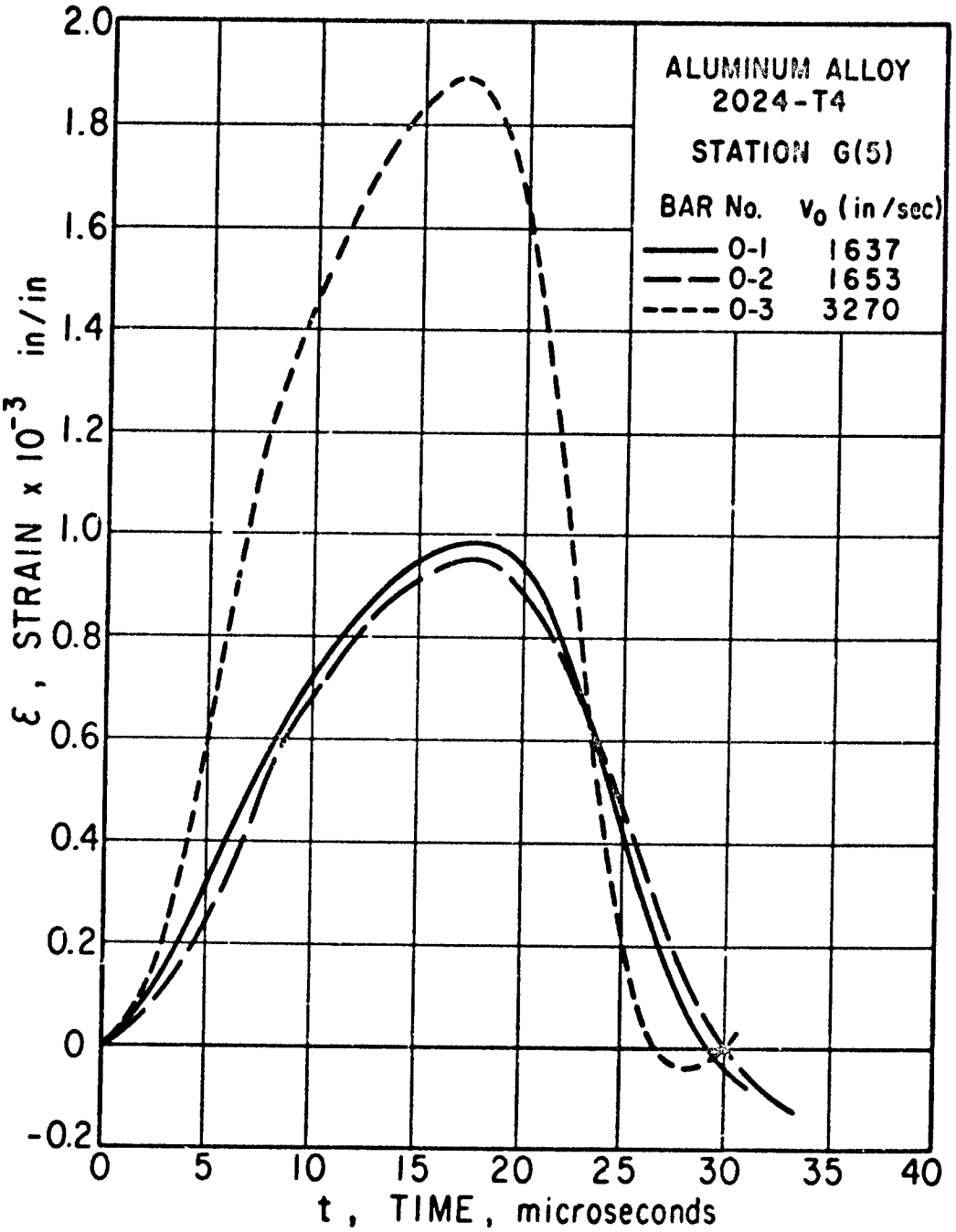

FIG. 31. Input Pulse Shapes Measured in the Aluminum Protector for Runs 0-1, 0-2, and 0-3 Produced by the Impact of a Hard-Steel Sphere ½-in. in Diameter.

that found for basalt but is slightly lower than the corresponding characteristic of the diorite.

The static test results for the shocked leucogranite are summarized in Table 7. The compressive strength of fresh leucogranite ranged from 28,300 to 32,800 psi. Shocked leucogranite showed variations ranging from no change to a 50% strength reduction. All of the samples with significant compressive strength loss came from the distal end of the test rods, indicating the susceptibility of the leucogranite to tensile wave damage. In view of the small number of samples studied, the data on Young's modulus in shocked leucogranite were too scattered to yield valid interpretations.

WAVE PROPAGATION VELOCITIES

The propagation velocities shown in Tables 8–10 are obtained by evaluating the time difference in the cross-over points of the rising portion of the principal pulse observed at two different strain-gage stations $10\frac{1}{2}$ inches apart. However, if alternative reference points on the pulse or other distances between the two strain-gage observation stations are chosen, different values of the wave velocity are calculated.

Table 11 shows the propagation velocities obtained by using different gage-station intervals and using the start of the chief pulse as the reference point. Table 12 shows the wave velocity obtained for leucogranite by using different strain-gage-station intervals as well as different reference points on the pulse. These reference points are: the start of the first deviation from the base line, the start of the principal pulse, and the peak of the principal pulse.

The nonuniformity of the apparent stress wave propagation velocity for a certain material depends upon the following four factors: instrumentation error, reading error, inhomogeneity of the test material, and wave dispersion. In these studies, the instrumentation error includes a 2% possible error due to gage measurement with an oscilloscope and a 1% possible error due to the gage factor. The reading error in these studies includes the error in determining the reference point and the error in reading the time scale. The percentage error in reading the time scale increases as the time difference decreases and is estimated to be about 12% for observations based on a $3\frac{1}{2}$-inch strain-gage-station interval and about 4% for observations based on a $10\frac{1}{2}$-inch strain-gage-station interval.

The observed velocities of wave propagation in spessartite, aluminum alloy, and basalt are much more uniform than the velocities observed in leucogranite and diorite, as shown in Table 11. The larger grain size of the leucogranite and diorite are presumed to be responsible for the larger variations in the measured wave velocity for these two materials.

TABLE 8. Summary of Dynamic Tests on 0.845-inch-Diameter Rods of Spessartite, Basalt, and Aluminum

Run no.	Previous shocks, no.	Distance, from impact end to 1st gage G(1), in.	Initial projectile velocity, in/sec	Strain amplitude of[a] initial pulse at station, 10^{-3} in/in					Wave[b] propagation velocity, 10^3 in/sec	Dynamic Young's modulus, psi x 10^{-6}	Material
				G(1)	G(2)	G(3)	G(4)	G(5)			
E-1	0	5.50	3,273	1.38	1.34	1.28	1.00	....	238.6	15.26	Spessartite
E-2	1	4.22	3,280	1.37	1.30	1.31	0.96	....	244.2	15.98	
E-3	2	2.51	3,270	1.42	1.36	1.36	0.88	....	262.5	18.47	
F-1	0	12.50	3,272	....	....	1.45	1.40	....	241.4	15.62	
F-6	5	6.00	3,288	....	....	1.41	1.39	....	259.3	18.02	
F-12	11	12.00	3,210	....	....	1.45	1.41	....	259.3	18.02	
H-1	0	5.52	3,252	1.41	1.47	1.42	1.44	1.36	244.1	15.96	
H-2	1	5.53	3,280	1.32	1.37	1.33	1.35	1.34	244.4	16.01	
H-3	2	5.50	3,270	1.34	1.40	1.34	1.38	1.36	244.1	15.96	
H-4	3	5.13	3,264	1.27	1.29	1.28	1.24	1.30	241.5	15.63	
H-5	4	5.50	3,247	1.42	1.41	1.33	1.36	1.33	231.0	14.30	
I-1	0	5.50	3,288	1.44	1.36	1.37	1.36	....	244.2	15.98	
I-2	1	4.08	3,280	1.55	1.54	1.49	1.49	....	244.2	15.98	
I-3	2	2.50	3,266	1.46	1.44	1.47	1.45	....	244.2	15.98	
X-3	..	7.65	3,270	1.77	....	....	1.77	....	214.2	11.88	Aluminum alloy 2024-T4
X-4	..	7.50	3,280	1.85	....	....	1.75	....	214.2	11.88	
Z	..	5.66	3,260	1.94	....	....	1.94	....	214.0	11.86	
J-1	0	5.50	3,282	1.78	1.68	1.52	1.47	....	191.0	9.23	Basalt
J-2	1	4.15	3,277	1.77	1.74	1.57	1.58	....	191.0	9.23	
J-3	2	2.83	3,273	1.96	1.88	1.76	1.72	....	171.5	7.44	
L-1	0	5.50	3,295	1.66	1.66	1.44	1.49	....	205.5	10.68	
L-2	1	4.08	3,279	1.80	1.80	1.59	1.62	....	198.0	9.92	
L-3	2	2.80	3,261	1.72	1.70	1.62	1.63	....	206.0	10.74	
M-1	0	12.50	3,257	....	....	1.61	1.40	....	194.5	9.57	
M-5	4	3.13	3,257	....	....	1.87	1.59	....	194.5	9.57	
M-10	9	9.46	3,259	....	....	1.96	1.93	....	184.2	8.58	

[a] All gages are 3½ inches apart.
[b] Obtained as the average of the total number of stations used for each run.

TABLE 9. Summary of Dynamic Tests on 0.845-inch-Diameter Rods of Leucogranite

Run no.	Previous shocks, no.	Distance, from impact end to 1st gage G(1), in.	Initial projectile velocity, in/sec	Strain amplitude of initial[a] pulse at station, 10^{-5} in/in					Wave[b] propagation velocity, 10^3 in/sec	Dynamic Young's modulus, psi x 10^{-6}
				G(1)	G(2)	G(3)	G(4)	G(5)		
0-1	0	8.03	1,637	1.94 1.95[c]	1.90	1.00	0.91	0.99	128.0	3.96
0-2	1	7.94	1,653	1.96 2.00[c]	1.60	0.93	0.93	0.95	115.4	3.22
0-3	2	7.78	3,270	3.48 3.48[c]	....	2.00	1.90	1.89	145.8	5.14
P-2	1	5.40	3,295	1.44 1.61[c]	1.38	0.85	0.54	....	135.5	4.18
P-3	2	6.60	3,252	....	1.12	0.70	0.47	....	130.0	4.09
P-4	3	9.15	3,260	0.92	1.02	0.64	0.45	....	133.0	4.28
Q-1	0	7.70	3,282	0.82 1.32[c]	0.62	0.39	0.31	....	136.3	4.50

NOTE: Specimen No. 0 has an aluminum alloy protector of the same diameter and a length of 5.81 in. at impact end; strain gage station G(5) is mounted on the aluminum protector in this particular case (see Fig. 16).

[a] All gages are $3\frac{1}{2}$ inches apart.

[b] Obtained as the average of the total number of stations used for each run.

[c] $\frac{1}{2}$-in.-long SR-4 wire resistance strain gage Type FA 50-12 was used here.

TABLE 10. Summary of Dynamic Tests on 3/4-inch-Diameter Rods of Diorite

Run no.	Previous shocks, no.	Distance, from impact end to 1st gage G(1), in.	Initial projectile velocity, in/sec	Strain amplitude of initial[a] pulse at station, 10^{-3} in/in					Wave[b] propagation velocity, 10^3 in/sec	Dynamic Young's modulus, psi x 10^6
				G(1)	G(2)	G(3)	G(4)	G(5)		
1	0	5.50	3,327	..82	....	0.56	0.56	0.18	144.5	5.50
2	1	4.34	3,253	2.26	1.06	0.68	0.59	0.20	131.5	4.53
3	0	5.19	3,294	1.69	....	....	0.65	....	144.2	5.46
4	0	5.13	3,291	1.54	....	....	0.39	....	144.4	5.33
5	0	5.54	3,294	1.59	....	....	0.99	....	144.8	5.51
6	1	6.00	3,289	1.55	....	....	1.25	....	142.5	5.35
7	2	4.05	3,275	2.01	....	....	0.68	....	143.0	5.36
8	3	3.88	3,181	1.85	....	....	0.76	....	104.0	2.84
9	4	2.50	3,291	1.77	....	....	1.02	....	106.8	3.00
10[c]	5	3.56	3,302	2.26	....	....	0.60	....	127.0	4.24
11[c]	0	5.50	3,211	2.44	....	....	1.16	....	144.8	5.51
12[c]	1	5.61	3,201	1.52	....	....	0.82	....	129.6	4.42
13[c]	1	5.62	3,215	2.70	....	....	1.00	....	131.3	4.54
14[c]	4	2.53	3,164	3.24	....	....	1.28	....	142.5	5.35
15[c]	5	3.12	3,167	3.72	....	....	1.52	....	104.0	2.84

[a] All gages are approximately 3½ inches apart.
[b] Obtained as the average of the total number of stations used for each run.
[c] Flat-nosed cylindrical projectile was used.

TABLE 11. Wave Propagation Velocity Between Different Stations

Material	Run no.	Propagation velocity between stations, 10^3 in/sec			
		G(1)-G(2)	G(2)-G(3)	G(3)-G(4)	G(1)-G(4)
Spessartite	E-1	233.3	269.2	218.8	238.6
	E-2	250.0	218.8	269.2	244.2
	E-3	233.3	269.2	291.7	262.5
	F-1	.....	.....	241.4	.....
	F-6	.....	.....	259.3	.....
	F-12	.....	.....	259.3	.....
	H-1	250.0	269.2	218.8	244.1
	H-2	245.0	269.3	218.8	244.4
	H-3	291.7	218.7	233.3	241.1
	H-4	241.4	250.0	233.3	241.5
	H-5	250.0	218.8	233.3	231.0
	I-1	250.0	250.0	233.3	244.2
	I-2	269.2	218.8	250.0	244.2
	I-3	250.0	233.3	250.0	244.2
Aluminum alloy 2024-T4	X-3	.....	.....	.....	214.2
	X-4	.....	.....	.....	214.2
	Z	.....	.....	.....	214.0
Basalt	J-1	200.0	175.0	200.0	191.0
	J-2	200.0	200.0	175.0	191.0
	J-3	200.0	175.0	155.6	171.5
	L-1	213.4	184.2	218.8	205.5
	L-2	205.9	194.4	194.4	198.0
	L-3	218.8	205.9	194.4	206.0
	M-1	.....	.....	194.5	.....
	M-5	.....	.....	194.5	.....
	M-10	.....	.....	184.2	.....
Leucogranite	O-1	125.0	145.8	116.7	128.0
	O-2	145.8	106.1	102.9	115.4
	O-3	142.9	.....	152.2	145.8
	P-2	132.0	143.0	132.0	135.5
	P-3	121.0	155.5	116.5	130.0
	P-4	125.0	143.0	132.0	133.0
	Q-1	116.5	159.0	140.0	136.3
Diorite	1	144.5	144.5	144.8	.....
	2	103.0	123.5	136.0	.....

TABLE 12. Velocity of Wave Propagation for Leucogranite Measured at Different Locations and Using Different Reference Points

Run no.	Measured between stations	Propagation velocities, 10^3 in/sec when reference point taken at		
		Initial deviation from base line	Start of principal pulse	Principal pulse peak
P-2	G(1)-G(2)	127.2	132.0	111.0
	G(2)-G(3)	175.0	143.0	149.0
	G(3)-G(4)	116.8	132.0	125.0
P-3	G(1)-G(2)	194.2	120.5	132.0
	G(2)-G(3)	104.2	155.2	146.0
	G(3)-G(4)	132.0	116.5	127.2
P-4	G(1)-G(2)	215.5	125.0	133.6
	G(2)-G(3)	125.0	143.0	132.0
	G(3)-G(4)	133.6	132.0	132.0

All of the rock rods were held to a constant diameter for a single rock material. Aluminum, however, was varied using the same alloy and was found to yield noticeably larger wave velocities with moderate increases in diameter. Aluminum rods 0.500, 0.750, and 0.845 inches in diameter exhibited velocities of 204,000, 205,400–210,000, and 214,000–214,200 ips, respectively.

STATIC AND DYNAMIC YOUNG'S MODULI

The dynamic Young's modulus for one-dimensional propagation in a bar is taken to be equal to $c_o^2\rho$ where c_o is the wave velocity in inches per second and ρ is the density of the material in pounds mass per cubic inch.[2] The values for the dynamic Young's modulus of the various materials tested have been summarized in Tables 8–10. The principal variations in the observed value of the dynamic Young's modulus for virgin materials with respect to their average values are found to be $\pm$ 1.7% for spessartite, $\pm$ 6.1% for basalt, $\pm$ 6.4% for leucogranite, and $\pm$ 1.5% for diorite. These figures represent the variations in the macroscopic distribution of constituent components and in geologic flaws along the rods tested. As an independent check on the dynamic Young's modulus for leucogranite, the

[2] This identity is theoretically exact for an infinitely thin rod of an ideally elastic material.

continuity conditions at the interface of the aluminum protector and the specimen were calculated for Run 0-1 using the measured rod wave velocity of 128,000 ips and a density of 0.000241 pounds mass per cubic inch, as well as the standard properties previously cited for the aluminum alloy employed. These calculations resulted in a dynamic Young's modulus of 3.98×10^6 psi for leucogranite, which is in complete accord with the value obtained from wave velocity measured. In general, the variations in the dynamic Young's moduli of virgin specimens were considerably smaller than the variations observed in the static Young's moduli of the same materials. This result is at least partially attributed to the fact that the stress wave, representing a rapidly applied moving load, would tend to minimize the effects of stress concentration, structural flaws, and other inhomogeneities that make static tests highly time-dependent.

SCHEMATIC COMPARISON OF PULSE PATTERNS

A schematic comparison of the pulse patterns obtained is presented in Fig. 32. The patterns for spessartite and basalt are almost exactly the same except for the slight attenuation at the test stress level observed in the basalt. Similarly, the pulse patterns for diorite and leucogranite are of the same type if the oscillations due to the coarse grains in the leucogranite are ignored. Both diorite and leucogranite yield a pulse with a steep rise, a long pulse duration, and considerable attenuation. There are also differences of a significant nature between these two materials. Leucogranite shows drastic oscillations, but the most remarkable difference is that the tensile-strain amplitude that results from distal-end reflection tends to attenuate in leucogranite as the reflected wave returns while in diorite the reflected wave tends to increase in amplitude as it returns.

CONCLUSIONS

Basalt shows slight attenuation and virtually no dispersion. Both the coefficient of attenuation and the Young's modulus for basalt tend to decrease as the number of shocks experienced by the specimen is increased. The strength of basalt did not appear to be affected by the pulse intensity employed in these tests and the basalt provides an excellent example of the ability of a brittle material to attain damage saturation with a given severity of repeated impacts.

Spessartite was found to be highly elastic, to exhibit virtually no attenuation and dispersion, and to be essentially unaffected by repeated stress wave passage with the pulse intensity employed in these tests.

Diorite possesses a high degree of attenuation but no dispersion. The ultimate strength of diorite and the static Young's modulus of diorite

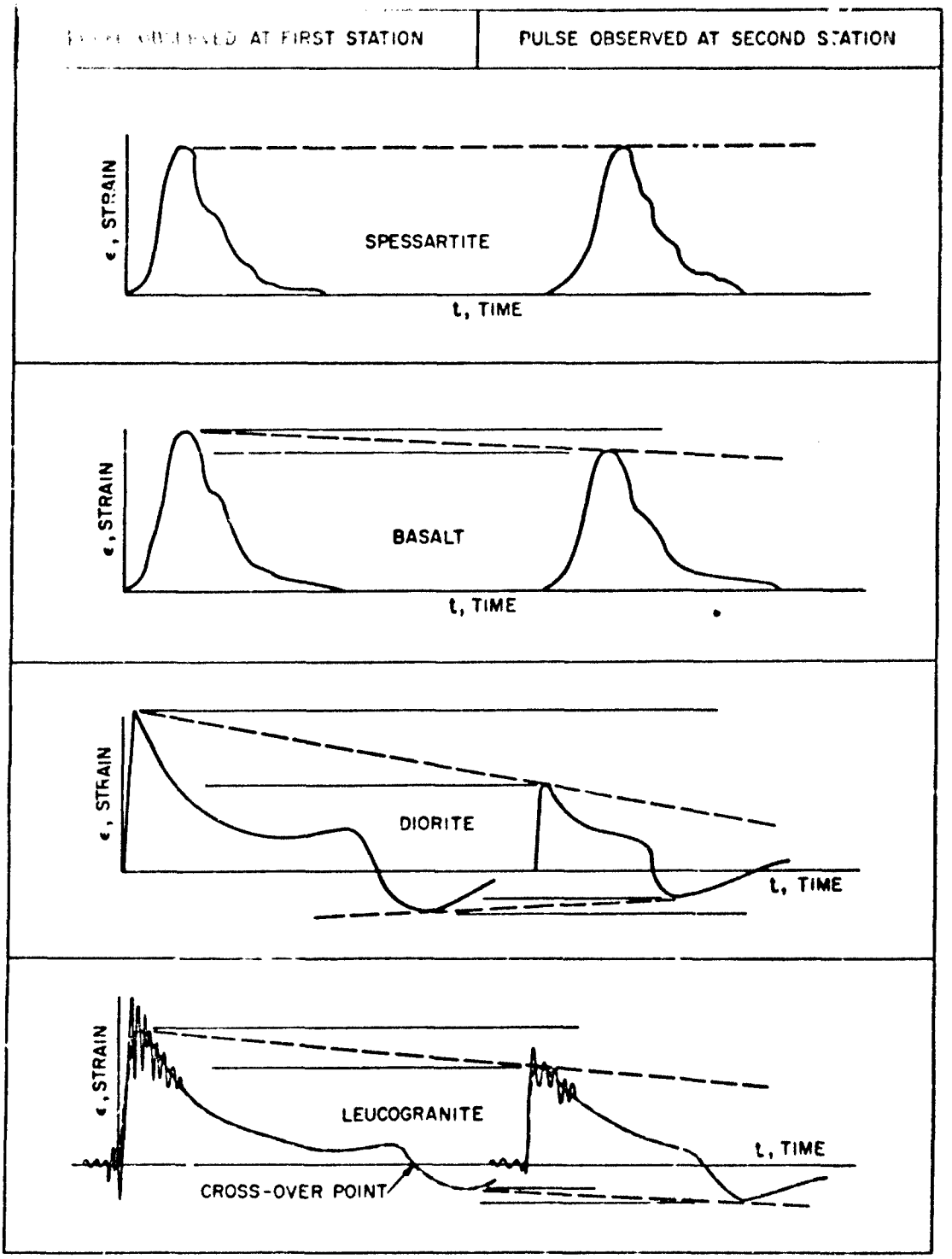

FIG. 32. Schematic Comparison of Pulse Patterns.

both decrease in direct proportion to the number of impact previously experienced by the specimen.

Leucogranite exhibits considerable attenuation and pulses in leucogranite exhibit drastic fluctuations at the pulse front. The compressive strength of leucogranite appears somewhat affected by the reflected tensile wave but did not appear influenced by the incident compressive wave.

The relative behavior of each material can be summarized as follows, when ranked according to the uniformity in dynamic response to the magnitude of impulse employed and to observed elastic characteristics:

spessartite - most elastic

basalt

diorite

leucogranite - least elastic

At one extreme, the spessartite below its fracture point behaves similarly to a metal; at the other extreme, the leucogranite was found to be definitely anelastic.

The various factors that appeared to affect the dynamic behavior of the igneous rocks tested are grain size, grain bond strength, and the effect of repetitive shocks. Large grain sizes lead to an increase in the attenuation, to local variations in the value of the rod wave velocity and in the dynamic Young's modulus, and also result in large oscillations in the pulse shape.

The weaker grain structure of the very coarse-grained rocks seemed to be a factor in the creation of both drastic fluctuations and attenuation of the pulse. Repeated shocks have a general tendency to decrease the value of Young's modulus and the ultimate strength except for those materials that follow a simple elastic model.

The rocks tested in this investigation are all typical brittle materials and no plastic deformation was observed in any of the test-rod failures. The smallest period of the transient pulse in the tests performed in this study was found to be 30 μsec for aluminum. To ensure that the value of $c/c_o > 0.99$, for the first mode of longitudinal motion and a harmonic pulse component of this period, the required size of the test rod was theoretically shown to be 0.98 inches in diameter or less. This study was restricted to test rods not larger than 0.845 inches in diameter, justifying the general conclusion that, confirmed experimentally in aluminum, the geometric dispersion could be neglected in the present case. For the current investigation, the probability of a single test being able to represent the statistical average properties of a given

rock type appears to be a function of grain size and the compactness of the texture, with the dynamic results generally more consistent than the static results.

The experimental data indicate that when a transient pulse with a stress level above a critical value traverses a rock rod, energy is absorbed by the rod in the form of fractures, grain cleavages, and damage to grain-to-grain bonds resulting from general comminution. A simple macroscopic model applicable to rock or to other granular brittle materials must therefore incorporate the effect of these significant phenomena. A solid friction mechanism appears to be definitely more applicable for a description of such materials than a viscoelastic model. This is particularly true at the high rates of loading encountered in the propagation of stress waves induced by impact or explosive loading, for under these conditions, the short duration of the pulses would not permit significant manifestations of time-dependent viscous phenomena. The general absence of dispersion observed in the rocks tested offers strong support for this conclusion.

A general conclusion, warranted by these studies, is that the response of brittle, granular solids should be analyzed directly, and not by analogies drawn from the behavior of metals or plastics. The specific studies reported in this investigation, although conducted on rock, offer more valid behaviorial analogies for other granular brittle materials than do most common engineering materials. Thus estimates of attenuation, saturation to damage from transient stress levels, wave shape, and extent of fracture in materials such as cast explosives or propellants should be more reasonable when based on granular rock behavior. Further, the studies in this report offer a number of areas for brittle solids technology that appear to warrant additional investigation.

REFERENCES

1. U. S. Naval Ordnance Test Station. Some Dynamic Characteristics of Rocks, by W. Goldsmith and C. F. Austin. China Lake, Calif., NOTS, May 1963. (NAVWEPS Report 8117, NOTS TP 3205). Also see Stress Waves in Anelastic Solids, ed. by Herbert Kolsky and William Prager, Berlin, Springer-Verlag, 1964, pp. 277-303.

2. Pochhammer, L. "Über die Fortpflanzungsgeschwindigkeiten kleiner Schwingungen in einem unbegrenzten isotropen Kreiszylinder," J REINE ANGEW MATH, Vol. 81 (1876), p. 324.

3. Chree, C. "The Equations of an Isotropic Elastic Solid in Polar and Cylindrical Coordinates, Their Solution and Application," CAMBRIDGE PHIL SOC, TRANS, Vol. 14 (1889), p. 250.

4. von Kármán, Th., and P. E. Duwez. "On the Propagation of Plastic Deformation in Solids," J APPL PHYS, Vol. 21 (1950), p. 987.

5. Taylor, G. I. "The Testing of Materials at High Rates of Loading," INST CIVIL ENGR (London), J, Vol. 26 (1946), p. 486.

6. Rahmatoolin, H. A. "On Plastic Waves of Loading," (in Russian), PRIK MAT MECH, Vol. 9 (1945), p. 91.

7. Kolsky, H. Stress Waves in Solids. Oxford, Clarendon, 1953.

8. Rinehart, J. S., and J. Pearson. Behavior of Metals under Impulsive Loads. Cleveland, ASM, 1954.

9. Goldsmith, W. Impact--The Theory and Physical Behavior of Colliding Solids. London, Arnold, 1960.

10. Redwood, M. Mechanical Waveguides. New York, Macmillan, 1960.

11. Rahmatoolin, H. A., and Y. A. Demyanov. Strength under Impulsive Loading (in Russian). Moscow, Natl. Publ. of Phys. Math. Lit., 1961.

12. Davies, R. M. "Stress Waves in Solids," in Surveys in Mechanics, ed. by George K. Batchelov and R. M. Davies. Cambridge, England, Cambridge Univ. Press, 1956. Pp. 64-138.

13. Abramson, H. N., H. J. Plass, and E. A. Ripperger. "Stress Wave Propagation in Rods and Beams," in Advances in Applied Mechanics. New York, Academic, 1958. Vol. 5, pp. 111-94.

14. Hopkinson, B. "A Method of Measuring the Pressure Produced in the Detonation of High Explosive or by the Impact of Bullets," ROY SOC LONDON, PHIL TRANS, Ser. A, Vol. 213 (1914), p. 437.

15. Landon, J. W., and H. Quinney. "Experiments with the Hopkinson Pressure Bar," ROY SOC LONDON, PROC, Ser. A, Vol. 103 (1923), p. 622.

16. Davies, R. M. "A Critical Study of the Hopkinson Pressure Bar," ROY SOC LONDON, PHIL TRANS, Ser. A, Vol. 240 (1948), pp. 375-457.

17. Rinehart, J. S. "Some Quantitative Data Bearing on the Scabbing of Metals under Explosive Attack," J APPL PHYS, Vol. 22 (1951), p. 555.

18. ------. "Surface Energy, A Mode for Energy Absorption during Impact," AM J PHYS, Vol. 21 (1953), pp. 305-7.

19. Kolsky, H., and Y. Y. Shi. "Fractures Produced by Stress Pulses in Glass-like Solids," PHYS SOC LONDON, PROC, Vol. 72 (1958), pp. 447-53.

20. U. S. Bureau of Mines. A Method of Determining Dynamic Tensile Strength of Rock at Minimum Loading, by L. O. Bacon. Pittsburgh, Penn., BUMINES, 1962. (R. I. 6067.)

21. Poulter Laboratories, Stanford Research Institute. Finite Amplitude Stress Wave in Rocks, by D. R. Grine. Menlo Park, Calif., SRI, 1959. (SRI Technical Report 012-59.)

22. Bruckshaw, J. M., and P. C. Mahanta. "The Variation of the Elastic Constants of Rocks with Frequency," PETROLEUM (January 1954), p. 14.

23. Attewell, P. B. "Response of Rocks to High Velocity Impact," MIN MET SOC AM, TRANS, Vol. 71 (1962), pp. 705-24.

24. Green, W. A. "Dispersion Relations for Elastic Waves in Bars," in Progress in Solid Mechanics. The Hague, North-Holland, 1960, Vol. 1, p. 225.

25. Onoe, M., H. D. McNiven, and R. D. Mindlin. "Dispersion of Axially Symmetric Waves in Elastic Rods," J APPL MECH (ASME, TRANS, Ser. E), Vol. 29 (1962), p. 729.

26. Ricker, N. "Form and Nature of Seismic Waves and the Structure of Seismograms," GEOPHYSICS, Vol. 5 (1940), p. 348.

27. ------. "The Form and Law of Propagation of Seismic Wavelets," GEOPHYSICS, Vol. 18 (1953), pp. 10-40.

28. McDonal, F. J., F. A. Angona, R. L. Mills, R. L. Sengbush, R. G. Van Nostrand, and J. E. White. "Attenuation of Shear and Compressional Waves in Pierre Shale," GEOPHYS, Vol. 23 (1958), p. 421.

29. Knopoff, L. "The Seismic Pulse in Materials Possessing Solid Friction, I: Plane Waves," SEISMOL SOC AM, BULL, Vol. 46 (1956), p. 175.

30. Knopoff, L., and G. J. F. MacDonald. "Attenuation of Small Amplitude Stress Wave in Solids," REV MOD PHYS, Vol. 30 (1958), p. 1178.

31. U. S. Naval Ordnance Test Station. Rocks That Occur as Brittle Solid Test Materials, by C. F. Austin and J. K. Pringle. China Lake, Calif., NOTS, July 1962. (NAVWEPS Report 7928, NOTS TP 2955.)

32. Goldsmith, W., and G. W. Norris, Jr. "Stresses in Curved Beams due to Transverse Impact," in Proceedings of the 3rd U. S. National Congress of Applied Mechanics. New York, ASME, 1958. P. 153.

33. Cunningham, D. M., and W. Goldsmith. "Short-time Impulses Produced by Longitudinal Impact," SOC EXPL STRESS ANAL, PROC, Vol. 16, No. 2 (1959), p. 153.

34. Goldsmith, W., and P. T. Lyman, Jr. "The Penetration of Hard-steel Spheres into Plane Metal Surfaces," J APPL MECH (ASME, TRANS, Ser. E), Vol. 27 (1960), p. 717.

35. Walsh, J. B. "The Effect of Cracks on the Uniaxial Elastic Compression of Rocks," J GEOPHYS RES, Vol. 70 (1965), p. 399.